Università degli Studi di Padova

Dipartimento di Matematica "Tullio Levi-Civita"

Corso di Laurea Triennale in Matematica

The Kuramoto Model as a Paradigm for Synchronization in Neural Systems

Relatore:
Prof. Marco Formentin

Candidato:
Francesca Rizzato
Matricola: 2032688

Anno accademico 2025/2026

24 Aprile 2026

Contents

Introduction **4**

1 Kuramoto Model: a model for synchronization **6**
1.1 Oscillatory systems and synchronization 6
1.2 From observations to theory 8
1.3 The Kuramoto model 9
1.3.1 Numerical validation for the phase transition 13
1.4 Proofs of the main results 15
1.4.1 Mean-field formulation 15
1.4.2 Stationary density 15
1.4.3 Self-Consistency Setup 16
1.4.4 Locked Phase Contribution 17
1.4.5 Drifting Phase Contribution 19
1.4.6 The Self-Consistency Equation and Critical Threshold 20
1.4.7 Bifurcation Scaling 22

2 Adaptive Synchronization in Neural Systems **24**
2.1 The Need for an Adaptive Model 24
2.2 Formalization of the Generalized Model 25
2.3 Architectures of Neural Connectivity 28
2.4 Numerical Analysis of Adaptive Synchronization 29
2.4.1 Effect of Static Coupling Strength 30
2.4.2 Effect of Dynamic Coupling Strength 34
2.4.3 Influence of Network Topology 38
2.4.4 Static Frequency Distribution 40
2.4.5 Time-Dependent Natural Frequencies 42
2.4.6 Combined Effects on Synchronization 43

Conclusions **46**

Appendix A: Python Codes **49**

Bibliography **67**

Introduction

The phenomenon of synchronization is central of a wide range of scientific disciplines, including physics, mathematics, biology, and neuroscience. As discussed by Pikovsky, Rosenblum, and Kurths [2], systems composed of many interacting oscillatory units often exhibit the spontaneous emergence of coherent collective behavior, even when the individual components are heterogeneous and only weakly coupled. Examples of such phenomena are widespread in natural and technological systems, ranging from the coordinated firing of neurons in the brain to the rhythmic contraction of cardiac pacemaker cells, circadian rhythms regulating biological clocks, and chemical oscillations. In medicine and physiology, synchronization plays a crucial role in normal functioning, while its disruption is often associated with pathological conditions such as cardiac arrhythmias, epilepsy, or Parkinsonian tremors.

To capture the emergence and breakdown of such collective rhythmic activity, several mathematical frameworks have been proposed. Among these, a paradigmatic approach for investigating synchronization is the Kuramoto model, introduced in the 1970s as a minimal formulation for phase synchronization in populations of coupled oscillators. As discussed in detail by Strogatz [1], despite its simplicity, the model captures essential features of collective dynamics, including the transition from an incoherent state to a synchronized regime. For this reason, the Kuramoto model has become fundamental in the theoretical study of synchronization phenomena.

The structure of this thesis is organized as follows.

Chapter 1: In the first chapter of this thesis, a detailed mathematical analysis of the Kuramoto model in the mean-field setting is presented. After introducing the model, the main results are stated and discussed, providing an overview of the qualitative behavior of the system. These results are then illustrated through numerical simulations, which highlight the transition from incoherent to synchronized regimes. Finally, proofs of the previously stated results are provided. Particular attention is devoted to the order parameter, the determination of the critical coupling strength at which synchronization

emerges, and the analysis of the associated bifurcation, following the classical treatment of Strogatz [1].

Chapter 2: In the second chapter, the focus shifts to applications of the Kuramoto model to neuronal synchronization. Neural activity in the brain is characterized by oscillations occurring at multiple spatial and temporal scales, and synchronization among neuronal populations is believed to play a fundamental role in cognitive processes such as perception, memory, and attention. Within this context, suitably generalized Kuramoto-type models provide a valuable conceptual framework for describing collective neuronal dynamics and for linking microscopic neuronal activity to macroscopic brain rhythms, as explored by Cumin and Unsworth [3]. Moreover, the discussion in this chapter is also supported by classical works on small-world architectures [5] and by the comprehensive review of Kuramoto dynamics by Acebrón et al. [4].

Chapter 1

Kuramoto Model: a model for synchronization

1.1 Oscillatory systems and synchronization

The main aim of this thesis is to understand the mechanisms underlying synchronization in natural phenomena. To this end, it is essential to clarify the notion of synchronization and to introduce the basic concepts related to oscillatory dynamics.

Synchronization is a collective phenomenon that emerges in systems composed of interacting oscillatory units and plays a central role in the dynamics studied in this thesis. Despite the wide variety of physical, biological, and technological systems in which it appears, synchronization often arises from common underlying mechanisms that can be described within a unified theoretical framework.
Before introducing the mathematical models and presenting the main results, we briefly outline the fundamental notions of oscillatory dynamics and synchronization that will be used throughout this chapter. This section is intended to fix terminology and intuition to understand the model we will analyze.

A paradigmatic example of an oscillatory system is provided by a pendulum clock. Its oscillatory motion is sustained by an internal energy source and persists independently of the specific initial conditions. This behavior exemplifies a broad class of systems known as self-sustained oscillators, which serve as the basic building blocks of the models considered in the following sections.

Definition 1.1 (Self-sustained oscillator)**.** *A self-sustained oscillator is a dynamical system capable of maintaining stable oscillations through an internal energy source,*

without requiring periodic external forcing. The amplitude and frequency of the oscillation are determined by the intrinsic properties of the system and are largely independent of the initial conditions.

Self-sustained oscillators share a number of characteristic features that are relevant for the study of collective dynamics.
First, their evolution is autonomous, as the energy required to sustain the oscillation is internally generated. Second, their oscillatory behavior depends on system-specific parameters, which determine their natural rhythm. Finally, their oscillations are stable with respect to small perturbations, allowing the system to return to its characteristic motion after being disturbed.

A key quantitative descriptor of an oscillatory system is its rhythm. For periodic motion, this is characterized by the period T, defined as the time required to complete one oscillation. The corresponding cyclic frequency is given by

$$f = \frac{1}{T},$$

while the angular frequency,

$$\omega = 2\pi f = \frac{2\pi}{T},$$

represents the natural frequency of the oscillator. In populations of oscillators, differences in natural frequencies play a crucial role in shaping the collective behavior.

When oscillators interact, even weak interactions can induce a coupling between oscillatory units, allowing the state of one oscillator to influence the evolution of others. In mechanical systems, such coupling may arise through a shared support or medium, while in more abstract settings it is modeled through explicit interaction terms in the equations of motion.
The presence of coupling opens the possibility of rhythm adjustment. Under suitable conditions, interacting oscillators with different natural frequencies may partially or fully align their rhythms over time. This process leads to the emergence of coherent collective behavior and is referred to as synchronization.

Definition 1.2 (Synchronization)**.** *Synchronization is a phenomenon that leads to the adjustment of rhythms of self-sustained periodic oscillators due to their weak interaction. In large populations, synchronization often manifests itself through non-equilibrium phase transitions between incoherent and coherent states.*

These considerations motivate a phase-based description of oscillatory systems, in which the state of each oscillator is represented by a single angular variable. This framework provides a natural setting for the analysis of large populations of coupled oscillators and forms the basis for the models, results, and numerical investigations presented in the remainder of this chapter.

1.2 From observations to theory

In this section, we trace the development of synchronization studies, starting from the first observations of the phenomenon to the more systematic theoretical approaches of the twentieth century.

Synchronization was first observed by Christiaan Huygens, a Dutch scientist who in the 17th-century realized that two pendulum clocks hung from a common, movable support (like a beam) would naturally synchronize their swings, due to weak mechanical vibrations transmitted through the support. He described this phenomenon as the "sympathy of two clocks" in a letter to his father.

A first systematic attempt to study collective synchronization was made around the mid-twentieth century by the American mathematician Norbert Wiener. He recognized the importance and ubiquity of synchronization in natural systems and attempted to describe these phenomena using a mathematical framework based on Fourier integrals. However, his analysis did not lead to a general nonlinear dynamical theory capable of describing the onset of collective synchronization.

A more fruitful contribution was given by Arthur T. Winfree, who focused on biological oscillators and proposed a general model for the collective synchronization of large populations of coupled phase oscillators. The dynamics of the system are described by

$$\dot{\theta}_i = \omega_i + \left(\sum_{j=1}^{N} X(\theta_j) \right) Z(\theta_i), \qquad i = 1, \ldots, N \tag{1.1}$$

where θ_i is the phase of oscillator i and ω_i its natural frequency. Each oscillator j exerts an influence $X(\theta_j)$ on all other oscillators and the related response of the i oscillator depends on the phase θ_i through the sensitivity function $Z(\theta_i)$. Despite the good intuition, this model is extremely general and mathematically challenging to analyze.

Winfree observed that the system behaves incoherently as long as the spread of natural frequencies remains large compared to the coupling strength. It is only when this spread

crosses a certain threshold that the incoherence breaks down and a subset of oscillators suddenly locks into synchrony. Namely, such oscillator populations can exhibit the temporal analog of a phase transition.

Building upon Winfree's ideas, Kuramoto began investigating the phenomenon in 1975. He introduced a simplified phase model with sinusoidal coupling, which will be the focus of the following sections.

1.3 The Kuramoto model

In this section, we introduce the mathematical model that will be used to describe the collective behavior of a population of interacting oscillators. We first present its final form and the type of dynamics it predicts, and only afterwards discuss the assumptions underlying its derivation.

We consider a population of self-sustained oscillators, namely dynamical systems possessing a stable limit cycle.

Definition 1.3 (Limit cycle)**.** *In the study of dynamical systems with two-dimensional phase space, a limit cycle is a closed trajectory in phase space such that nearby trajectories spiral into it either as time approaches infinity or as time approaches negative infinity. Stable limit cycles arise in many nonlinear systems and provide a natural description of self-sustained oscillations observed in real-world phenomena.*

Definition 1.4 (Stability of the limit cycle.)**.** *A limit cycle is called* stable *(or* attracting*) if small perturbations of the trajectory do not grow. More precisely, a limit cycle* Γ *is stable if there exists a neighborhood* U *of* Γ *such that every trajectory starting in* U *converges back to* Γ *as* $t \to +\infty$*. This property ensures that the amplitude of the oscillation remains bounded and close to the periodic orbit.*

When weak interactions between oscillators are introduced, their amplitudes remain close to the limit cycle and only the phases evolve over long time scales. Under this phase reduction, the most general form of the interaction between oscillators is described by

$$\dot{\theta}_i = \omega_i + \sum_{j=1}^{N} \Gamma_{ij}(\theta_j - \theta_i), \qquad i = 1, \dots, N, \tag{1.2}$$

where ω_i is the natural frequency of oscillator i and Γ_{ij} is an interaction function determined by the microscopic dynamics of the original system. Since the connection

topology and interaction functions are complex to analyze, we introduce a mean-field approximation. This assumes that each oscillator interacts with all others through an equally weighted, fully connected, and purely sinusoidal coupling. As a consequence, the many-body interaction is replaced by an effective averaged interaction and the coupling takes the sinusoidal form

$$\Gamma_{ij}(\theta_j - \theta_i) = \frac{K}{N}\sin(\theta_j - \theta_i), \tag{1.3}$$

where $K \geq 0$ represents the coupling strength and the scaling factor $1/N$ ensures a well-defined limit as $N \to \infty$.

Definition 1.5 (Governing equations of Kuramoto Model)**.** *The Kuramoto model describes a population of N coupled phase oscillators through the equations*

$$\dot{\theta}_i = \omega_i + \frac{K}{N}\sum_{j=1}^{N}\sin(\theta_j - \theta_i), \qquad i = 1, \ldots, N, \tag{1.4}$$

where $K \geq 0$ represents the coupling strength. The quantities ω_i denote the natural frequencies of the oscillators, and we assume that they are sampled from a probability density $g(\omega)$.

We adopt Kuramoto's classical assumptions, requiring $g(\omega)$ to be unimodal and symmetric with respect to its mean value Ω. By shifting to a rotating reference frame $\theta_i \mapsto \theta_i + \Omega t$, we can set the mean frequency to zero. Consequently, the transformed distribution is an even function, satisfying $g(\omega) = g(-\omega)$.

In order to gain a clearer understanding of the collective dynamics of the phases, it is convenient to rewrite the governing equations in a form that highlights the macroscopic behavior of the system. To this end, we introduce the complex order parameter.

Definition 1.6 (The complex order parameter)**.** *The complex order parameter is a macroscopic quantity that gives us information about the collective rhythm of the whole population. Its expression is*

$$re^{i\psi} = \frac{1}{N}\sum_{j=1}^{N} e^{i\theta_j}, \tag{1.5}$$

where $r \in [0, 1]$ measures the level of synchronization and ψ is the average phase.

Geometrically, the order parameter is the centroid of N unit vectors on the unit circle. A value of $r \approx 0$ corresponds to an incoherent regime with uniformly distributed phases, whereas $r \approx 1$ indicates a fully synchronized regime, as we can see in Figure 1.1.

Definition 1.7 (Incoherent state)**.** *A configuration of phases is said to be in an incoherent state (it presents an incoherent solution) if the phases are uniformly distributed on the unit circle. In this regime, the order parameter has magnitude* $r \approx 0$*. No macroscopic phase coherence emerges.*

Definition 1.8 (Synchronized state)**.** *A configuration is said to be in a synchronized state if a non-negligible fraction of oscillators share approximately the same phase. In this case, the order parameter satisfies* $r > 0$*, indicating the emergence of collective phase coherence.*

By rewriting the governing equations in terms of the order parameter, we obtain

$$\dot{\theta}_i = \omega_i + Kr\sin(\psi - \theta_i), \qquad i = 1, \dots, N. \tag{1.6}$$

In this formulation, each oscillator is effectively coupled to the mean field, with a coupling strength proportional to the coherence r.

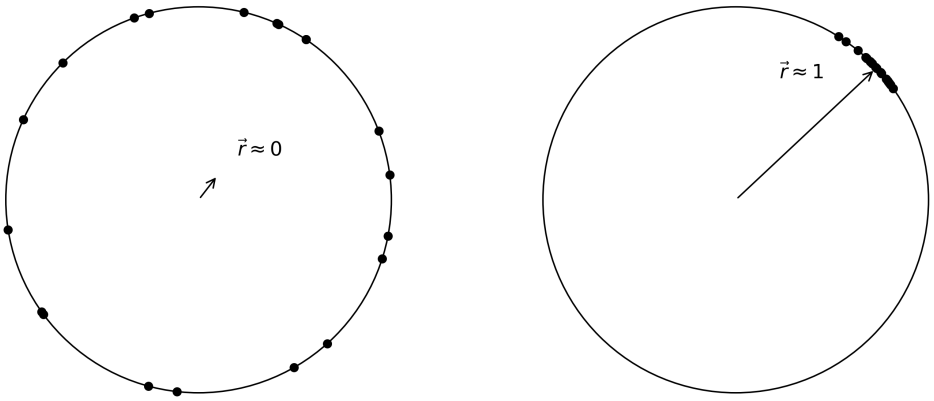

Figure 1.1: The oscillators are represented as points on the unit circle, identified by their phases. The magnitude $r \in [0, 1]$ *of the complex order parameter quantifies the level of phase coherence in the population. For* $r \approx 0$*, the phases are evenly spread and no collective behavior emerges (incoherent state). For* $r \approx 1$*, a macroscopic fraction of oscillators share approximately the same phase, signaling the onset of synchronization.*

In the limit $N \to \infty$, the mean-field description becomes exact. Moreover, the collective phase ψ can be set to zero without loss of generality by moving to a rotating reference frame. In this frame, the long-time dynamics of each oscillator is determined by the

competition between its natural frequency ω_i and the effective coupling strength Kr, which encodes the influence of the population. This leads to two qualitatively different asymptotic behaviors, summarized in the following proposition [1].

Proposition 1.9 (Classification of oscillators)**.** *In the thermodynamic limit, the population of oscillators partitions into two distinct groups based on their natural frequencies:*

1. *Locked oscillators: those with $|\omega_i| \leq Kr$. They approach a stable fixed point given by $\omega_i = Kr \sin \theta_i$ with $|\theta_i| \leq \frac{\pi}{2}$;*
2. *Drifting oscillators: those with $|\omega_i| > Kr$. They do not admit fixed points and continuously drift around the unit circle.*

The transition from an incoherent state to a synchronized one occurs when the coupling strength K exceeds a specific threshold that depends on the shape of the frequency distribution.

Proposition 1.10 (Critical coupling)**.** *Assume that the frequency distribution $g(\omega)$ is even, unimodal and smooth. Then the incoherent solution loses stability at the critical coupling*

$$K_c = \frac{2}{\pi g(0)}. \tag{1.7}$$

We now want to analyze the behavior of the synchronized branch in a neighborhood of critical coupling K_c. When a branch of stable synchronized solutions emerges continuously from the incoherent state as K crosses the critical value K_c, the bifurcation is said to be *supercritical*. In this case, the order parameter r grows smoothly from zero, typically following a square-root scaling. Conversely, if the synchronized branch exists for $K < K_c$ and is unstable at its onset, while a stable branch appears only for $K > K_c$ after a finite jump in r, the bifurcation is called *subcritical*.

In the Kuramoto model, the sign of the second derivative $g''(0)$ of the frequency distribution determines which of these two scenarios occurs. We formalize the result in Proposition 1.11.

Proposition 1.11 (Bifurcation of synchronized solutions)**.** *Let $g(\omega)$ be twice differentiable in $\omega = 0$. In a neighborhood of K_c, the order parameter scales as*

$$r \approx \sqrt{\frac{16}{\pi K_c^3}} \sqrt{\frac{\mu}{-g''(0)}}, \tag{1.8}$$

where $\mu = (K - K_c)/K_c$ represents the reduced coupling strength. In particular, the bifurcation is supercritical if $g''(0) < 0$ and subcritical if $g''(0) > 0$, since the sign of $g''(0)$ determines whether the emerging branch of synchronized solutions is stable or unstable at onset.

The proofs of the previous propositions and the detailed derivations leading to these results will be presented in Section 1.4. However, before delving into the formal mathematical treatment, we provide a numerical validation of the synchronization transition and the predicted bifurcation scaling through direct integration of the governing equations.

1.3.1 Numerical validation for the phase transition

In this section, we perform numerical simulations of the Kuramoto model to investigate the dynamical onset of synchronization and to validate the analytical predictions stated above. Specifically, we aim to numerically verify the emergence of the phase transition by simulating a population of oscillators whose natural frequencies follow a Lorentzian distribution.

Definition 1.12. *[Lorentzian distribution] A random variable ω is said to follow a Lorentzian (Cauchy) distribution with width parameter $\gamma > 0$ if its probability density function is*

$$g(\omega) = \frac{\gamma}{\pi(\omega^2 + \gamma^2)}.$$

The distribution is symmetric about zero and satisfies $g(0) = \frac{1}{\pi\gamma}$. Therefore, according to the theoretical result in Equation (1.7), the critical coupling strength for the onset of synchronization becomes $K_c = 2\gamma$.

To illustrate the bifurcation, we simulated a system of 10000 oscillators using the explicit Euler method with a time step $dt = 0.01$. The initial phases $\theta_i(0)$ were uniformly distributed in the interval $[0, 2\pi]$ to represent a fully incoherent initial state. The natural frequencies ω_i were sampled from a Lorentzian distribution with width parameter $\gamma = 1$, corresponding to the theoretical threshold of $K_c = 2.0$.

The system was evolved for 20 iterations to ensure convergence to a stationary regime. To mitigate finite-size effects and reduce intrinsic fluctuations, the stationary order parameter r for each coupling strength K was computed by averaging the results over 20 independent realizations. For the Lorentzian distribution, a direct computation

shows that

$$g''(0) = -\frac{2}{\pi\gamma^3} < 0.$$

Therefore, according to Proposition 1.11, the synchronization transition is supercritical. As shown in Figure 1.2, the numerical results are in good agreement with the theoretical predictions. In particular, for $K > K_c$, the order parameter r grows continuously from zero and exhibits the square-root scaling of the order parameter above the critical threshold.

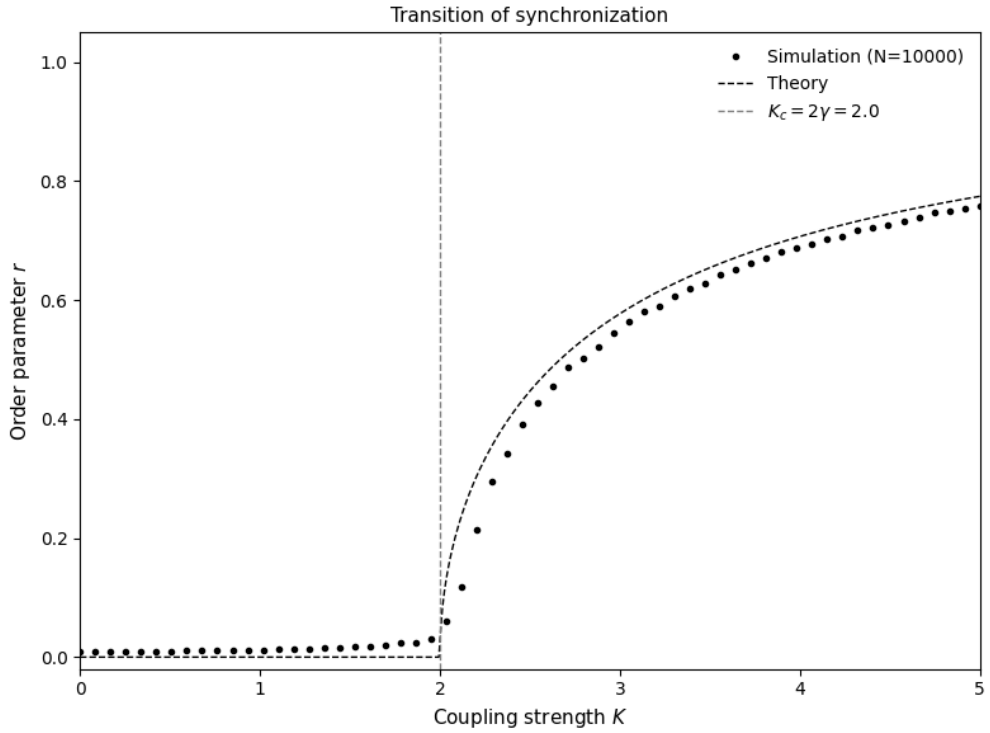

Figure 1.2: Synchronization phase transition in a population of $N = 10000$ oscillators with Lorentzian natural frequencies ω_i with width parameter $\gamma = 1$. The plot illustrates the stationary order parameter r as a function of the coupling strength K. Numerical results (black dots) were obtained using the explicit Euler method with a time step $dt = 0.01$, evolving the system for 20 iterations to reach a stationary regime and averaging over 20 independent realizations. The theoretical prediction identifies the critical coupling threshold at $K_c = 2\gamma = 2.0$ Above this threshold, a macroscopic synchronized state emerges ($r > 0$).

1.4 Proofs of the main results

This section collects detailed derivations of the results stated in Section 1.3. Specifically, we are going to derive the system of Equations (1.6). Then we will analyze in detail what Proposition 1.9 states. Finally, we are going to give proofs of Proposition 1.10 and Proposition 1.11.

1.4.1 Mean-field formulation

First of all, we want to derive the Equations (1.6). In order to do this, we need to rewrite Equations (1.4) in terms of the order parameter. We multiply both sides of the order parameter Equation (1.5) by $e^{-i\theta_i}$, obtaining:

$$re^{i\psi}e^{-i\theta_i} = \frac{1}{N}\sum_{j=1}^{N} e^{i\theta_j}e^{-i\theta_i} \tag{1.9}$$

$$re^{i(\psi-\theta_i)} = \frac{1}{N}\sum_{j=1}^{N} e^{i(\theta_j-\theta_i)}. \tag{1.10}$$

By equating imaginary parts, we get:

$$r\sin(\psi-\theta_i) = \frac{1}{N}\sum_{j=1}^{N}\sin(\theta_j-\theta_i) \tag{1.11}$$

Hence, the governing equations become:

$$\dot{\theta}_i = \omega_i + Kr\sin(\psi-\theta_i) \qquad i = 1,\dots,N, \tag{1.12}$$

that is exactly (1.6).

1.4.2 Stationary density

To analytically derive the self-consistency equation for r, we consider the thermodynamic limit $N \to \infty$. In this regime, the state of the system is no longer described by individual phases θ_i, but by a probability density function $\rho(\theta, \omega, t)$, representing the fraction of oscillators with natural frequency ω that have phase θ at time t. We look for a stationary state, where the global order parameter r and the phase ψ are constant. In such a state, the density must satisfy the continuity equation $\frac{\partial\rho}{\partial t} + \frac{\partial}{\partial\theta}(\rho\dot{\theta}) = 0$. Since we are in a stationary regime ($\frac{\partial\rho}{\partial t} = 0$), the product $\rho\dot{\theta}$ must be constant in θ.

Proposition 1.13 (Stationary density of drifting oscillators)**.** *Consider the Kuramoto model in the mean-field formulation and assume a stationary regime with constant order parameter r. For oscillators with $|\omega| > Kr$, the phase does not converge to a fixed point but keeps evolving in time. The corresponding stationary phase density is given by*

$$\rho(\theta, \omega) = \frac{C(\omega)}{|\omega - Kr \sin\theta|}, \tag{1.13}$$

where the normalization constant $C(\omega)$ is determined by the condition

$$\int_{-\pi}^{\pi} \rho(\theta, \omega)\, d\theta = 1. \tag{1.14}$$

In the general treatment of the model we define the stationary density of drifting oscillators (1.13) with condition (1.14) on the constant we are now going to make explicit.

For each ω, we get

$$\int_{-\pi}^{\pi} \rho(\theta, \omega) d\theta = \int_{-\pi}^{\pi} \frac{C}{|\omega - Kr \sin\theta|} d\theta \tag{1.15}$$

We are considering drifting oscillators, so, since $|\omega_i| > Kr$, it holds that $\omega - Kr \sin\theta > 0$. Thanks to this fact, we can remove the absolute value without loss of generality, getting:

$$\int_{-\pi}^{\pi} \frac{C}{|\omega - Kr \sin\theta|} d\theta = C \int_{-\pi}^{\pi} \frac{1}{\omega - Kr \sin\theta} d\theta = C \frac{2\pi}{\sqrt{\omega^2 - (Kr)^2}} \tag{1.16}$$

By imposing condition (1.14), we find:

$$C \frac{2\pi}{\sqrt{\omega^2 - (Kr)^2}} = 1 \tag{1.17}$$

from which we obtain

$$C = \frac{\sqrt{\omega^2 - (Kr)^2}}{2\pi} \tag{1.18}$$

1.4.3 Self-Consistency Setup

The population of oscillators naturally splits into two groups based on their natural frequency ω relative to the coupling strength Kr.

- *Locked oscillators* ($|\omega| \leq Kr$): These units have natural frequencies 'slow' enough to be captured by the mean field. They reach a stable fixed point $\dot{\theta} = 0$ where they all rotate at the same average speed, effectively 'freezing' their phase relative to the collective. They are the primary contributors to the order parameter r.

- *Drifting oscillators* ($|\omega| > Kr$): These units have natural frequencies that exceed the maximum coupling force. They can never reach a fixed point and instead 'drift' or rotate continuously along the unit circle. While they do not synchronize perfectly, they contribute to r through the non-uniformity of their speed (they spend more time at phases where $\dot{\theta}$ is small).

Observation 1.14. *From now on, angle brackets $\langle\cdot\rangle$ will be used to denote population averages taken in the limit $N \to \infty$.*

We now impose the self-consistency condition on the order parameter, requiring that its stationary value coincides with the one generated by the asymptotic phase distribution described in equations (1.6). We have the following:

$$\langle e^{i\theta} \rangle = \langle e^{i\theta} \rangle_{\text{lock}} + \langle e^{i\theta} \rangle_{\text{drift}} \tag{1.19}$$

The Kuramoto model exhibits rotational invariance: shifting all phases by the same constant does not change the dynamics. This symmetry allows us to move to a co-rotating reference frame, in which the average motion of the oscillators is removed.

In this frame, we can choose the orientation of the axes so that the average phase ψ of the population is aligned with the real axis. Therefore, without loss of generality, we set $\psi = 0$. As a result, the complex order parameter $re^{i\psi}$ reduces to the real quantity r, so $\langle e^{i\theta} \rangle = re^{i\psi} = r$. As a result, the order parameter can be written as the sum of two contributions,

$$r = \langle e^{i\theta} \rangle_{\text{lock}} + \langle e^{i\theta} \rangle_{\text{drift}} \tag{1.20}$$

In the following subsection, we are going to analyze how the two types of oscillators contribute to the order parameter, namely what is written in the Proposition 1.9

1.4.4 Locked Phase Contribution

Let us start by considering the contribution of locked oscillators. In the locked state, the phase of each oscillator converges to a stationary value θ^* that satisfies, for all $|\omega| \leq Kr$,

$$\sin \theta^* = \frac{\omega}{Kr}. \tag{1.21}$$

By using Euler's formula, we can rewrite the contribution $\langle e^{i\theta} \rangle_{\text{lock}}$ in (1.20) as

$$\langle e^{i\theta} \rangle_{\text{lock}} = \langle \cos\theta + i \sin\theta \rangle_{\text{lock}} = \langle \cos\theta \rangle_{\text{lock}} + i \langle \sin\theta \rangle_{\text{lock}} \tag{1.22}$$

In the limit for $N \to \infty$, the distribution of locked phases is determined by the one of natural frequencies $g(\omega)$. Since $g(\omega)$ is assumed to be an even function, i.e. $g(\omega) =$

$g(-\omega)$, the corresponding phase distribution is symmetric with respect to $\theta = 0$. As a consequence, the imaginary part of the average $\langle e^{i\theta} \rangle_{\text{lock}}$, namely $i\langle \sin\theta \rangle_{\text{lock}}$, vanishes. We can now show it as follows.

Proposition 1.15. *For the population of phase-locked oscillators, it holds that*

$$\langle \sin\theta \rangle_{lock} = 0 \tag{1.23}$$

Proof.

$$\begin{aligned}\langle \sin\theta \rangle_{\text{lock}} &= \int_{-Kr}^{Kr} \sin\theta(\omega)\, g(\omega)\, d\omega \\ &= \int_{-Kr}^{0} \sin\theta(\omega)\, g(\omega)\, d\omega + \int_{0}^{Kr} \sin\theta(\omega)\, g(\omega)\, d\omega.\end{aligned}$$

In the first integral we change the variable $\omega \mapsto -\omega$, which yields

$$\int_{-Kr}^{0} \sin\theta(\omega)\, g(\omega)\, d\omega = -\int_{0}^{Kr} \sin\theta(-\omega)\, g(-\omega)\, d\omega.$$

Using the evenness of the frequency distribution $g(\omega)$ and the antisymmetry $\theta(-\omega) = -\theta(\omega)$ for locked oscillators, we find

$$\begin{aligned}\langle \sin\theta \rangle_{\text{lock}} &= \int_{0}^{Kr} \big[-\sin\theta(-\omega) + \sin\theta(\omega)\big]\, g(\omega)\, d\omega \\ &= \int_{0}^{Kr} \big[-(-\sin\theta(\omega)) + \sin\theta(\omega)\big]\, g(\omega)\, d\omega = 0\end{aligned}$$

□

Thanks to this result, the contribution of locked oscillators reduces to the average of $\cos\theta$,

$$\langle e^{i\theta} \rangle_{\text{lock}} = \langle \cos\theta \rangle_{\text{lock}}. \tag{1.24}$$

This average can be expressed as an integral over the natural frequencies,

$$\langle e^{i\theta} \rangle_{\text{lock}} = \int_{-Kr}^{Kr} \cos\theta(\omega)\, g(\omega)\, d\omega, \tag{1.25}$$

where $\theta(\omega)$ is implicitly defined by $\omega_i = Kr\sin\theta_i$.
By changing the variable $\omega = Kr\sin\theta$, we get

$$\begin{aligned}\langle e^{i\theta}\rangle_{\text{lock}} &= Kr\int_{-\frac{\pi}{2}}^{\frac{\pi}{2}} \cos\theta\, g(Kr\sin\theta)\; Kr\cos\theta d\theta \\ &= Kr\int_{-\frac{\pi}{2}}^{\frac{\pi}{2}} \cos^2\theta\, g(Kr\sin\theta)\, d\theta.\end{aligned}$$

1.4.5 Drifting Phase Contribution

We now consider the contribution of the drifting oscillators, namely those with $|\omega| > Kr$. Unlike the locked oscillators, their phases do not converge to a fixed value but keep evolving in time. In the stationary regime, their contribution to the order parameter must therefore be computed by averaging over the corresponding invariant phase density $\rho(\theta,\omega)$.

The contribution of the drifting oscillators to the order parameter is given by

$$\langle e^{i\theta}\rangle_{\text{drift}} = \int_{|\omega|>Kr}\int_{-\pi}^{\pi} e^{i\theta}\,\rho(\theta,\omega)\,g(\omega)\,d\theta\,d\omega \tag{1.26}$$

This integral turns out to vanish because of the symmetry properties of the system. Indeed, the frequency distribution is even, $g(\omega) = g(-\omega)$, and the stationary density of drifting oscillators satisfies the symmetry relation

$$\rho(\theta+\pi,-\omega) = \rho(\theta,\omega) \tag{1.27}$$

This result is formalized in the following proposition.

Proposition 1.16 (Contribution of drifting oscillators)**.** *The contribution of drifting oscillators to the complex order parameter vanishes, namely*

$$\langle e^{i\theta}\rangle_{\text{drift}} = 0. \tag{1.28}$$

As a direct consequence of the previous result, only the population of phase-locked oscillators contributes coherently to the order parameter.

Corollary 1.17. *The stationary value of the order parameter is entirely determined by the locked oscillators.*

Proof of Proposition 1.16. We start from the definition

$$\langle e^{i\theta} \rangle_{\text{drift}} = \int_{|\omega|>Kr} \int_{-\pi}^{\pi} e^{i\theta}\, \rho(\theta,\omega)\, g(\omega)\, d\theta\, d\omega.$$

By splitting the integral over positive and negative frequencies, we get:

$$\begin{aligned}\langle e^{i\theta} \rangle_{\text{drift}} &= \int_{\omega>Kr} \int_{-\pi}^{\pi} e^{i\theta}\, \rho(\theta,\omega)\, g(\omega)\, d\theta\, d\omega + \int_{\omega<-Kr} \int_{-\pi}^{\pi} e^{i\theta}\, \rho(\theta,\omega)\, g(\omega)\, d\theta\, d\omega \\ &= \int_{Kr}^{+\infty} \int_{-\pi}^{\pi} e^{i\theta}\, \rho(\theta,\omega)\, g(\omega)\, d\theta\, d\omega + \int_{-\infty}^{-Kr} \int_{-\pi}^{\pi} e^{i\theta}\, \rho(\theta,\omega)\, g(\omega)\, d\theta\, d\omega\end{aligned}$$

In the last integral we can change the variables $\omega \mapsto -\omega$ and $\theta \mapsto \theta + \pi$. Since $d\theta$ and $d\omega$ are invariant under this transformation, we obtain

$$\begin{aligned}\int_{Kr}^{+\infty} \int_{-\pi}^{\pi} e^{i\theta}\, \rho(\theta,\omega)\, g(\omega)\, d\theta\, d\omega &= \int_{Kr}^{+\infty} \int_{-\pi}^{\pi} e^{i(\theta+\pi)}\, \rho(\theta+\pi,-\omega)\, g(-\omega)\, d\theta\, d\omega \\ &= -\int_{Kr}^{+\infty} \int_{-\pi}^{\pi} e^{i\theta}\, \rho(\theta,\omega)\, g(\omega)\, d\theta\, d\omega.\end{aligned}$$

In the last step we exploited the symmetry properties $g(-\omega) = g(\omega)$ and $\rho(\theta+\pi,-\omega) = \rho(\theta,\omega)$, and the fact that $e^{i(\theta+\pi)} = -e^{i\theta}$. So, substituting this last result into

$$\langle e^{i\theta} \rangle_{\text{drift}} = \int_{Kr}^{+\infty} \int_{-\pi}^{\pi} e^{i\theta}\, \rho(\theta,\omega)\, g(\omega)\, d\theta\, d\omega + \int_{-\infty}^{-Kr} \int_{-\pi}^{\pi} e^{i\theta}\, \rho(\theta,\omega)\, g(\omega)\, d\theta\, d\omega$$

we get:

$$\langle e^{i\theta} \rangle_{\text{drift}} = \int_{Kr}^{+\infty} \int_{-\pi}^{\pi} e^{i\theta}\, \rho(\theta,\omega)\, g(\omega)\, d\theta\, d\omega - \int_{Kr}^{+\infty} \int_{-\pi}^{\pi} e^{i\theta}\, \rho(\theta,\omega)\, g(\omega)\, d\theta\, d\omega$$

Therefore, the contributions from positive and negative drifting frequencies cancel exactly, yielding

$$\langle e^{i\theta} \rangle_{\text{drift}} = 0.$$

□

1.4.6 The Self-Consistency Equation and Critical Threshold

To complete the derivation of Proposition 1.10, the last fundamental step is the calculation of the value of K_c. To this end, we will analyze the self-consistency equation in the limit where the order parameter r tends to zero.

Collecting the results obtained for locked and drifting oscillators, we conclude that only the phase-locked population contributes to the order parameter. Indeed, the contribution of drifting oscillators vanishes by symmetry, while the locked oscillators yield a nonzero contribution through their stationary phases. As a consequence, the self-consistency condition for the order parameter reduces to the contribution of the locked oscillators alone, namely

$$r = Kr \int_{-\pi/2}^{\pi/2} \cos^2\theta \, g(Kr \sin\theta) \, d\theta \tag{1.29}$$

For any K, $r = 0$ solves this equation. In this case, for all angles θ and frequencies ω, the state is

$$\rho(\theta, \omega) = \frac{1}{2\pi} \tag{1.30}$$

This state is called the *incoherent state*, since the solution $r = 0$ corresponds to the lack of collective coherence among the oscillators and identifies a first branch of solutions.

If we instead look for non trivial solutions of (1.29),by assuming $r \neq 0$, we can divide both sides of the equation by r and we get

$$1 = K \int_{-\frac{\pi}{2}}^{\frac{\pi}{2}} \cos^2\theta \, g(Kr \sin\theta) \, d\theta. \tag{1.31}$$

We now want to take the limit for $r \to 0^+$ in integral (1.31).
In order to do this, we first need to write $\cos^2\theta$ in a better way. We use the cosine duplication formula to find

$$\cos^2\theta = \frac{\cos 2\theta + 1}{2} \tag{1.32}$$

and substituting it into (1.31) we get:

$$1 = \frac{\pi K g(0)}{2}. \tag{1.33}$$

The second branch of solutions continuously bifurcates from $r = 0$ at the value $K_c = K$ we just found:

$$K_c = \frac{2}{\pi g(0)}, \tag{1.34}$$

that is exactly the result we had seen in Proposition 1.10.

For $K < K_c$, the only stable solution is $r = 0$, corresponding to an incoherent state in which the oscillators evolve independently. At $K = K_c$, a continuous phase transition occurs and a nontrivial synchronized solution with $r > 0$ emerges.

1.4.7 Bifurcation Scaling

We now analyze the behavior of the order parameter r in a neighborhood of the critical coupling $K_c = \frac{2}{\pi g(0)}$ to show the Proposition 1.11. Recall the self-consistency equation for the synchronized branch (1.31),

$$1 = K \int_{-\frac{\pi}{2}}^{\frac{\pi}{2}} \cos^2\theta \, g(Kr\sin\theta)\, d\theta. \tag{1.35}$$

To determine the nature of the bifurcation at $K = K_c$, we expand the integrand for a small r. Since the frequency distribution $g(\omega)$ is assumed to be smooth, even, and unimodal, it admits a Taylor expansion around $\omega = 0$. We can write it as

$$g(\omega) = g(0) + \frac{1}{2} g''(0)\, \omega^2 + O(\omega^4) \tag{1.36}$$

where all odd derivatives vanish by symmetry.

Substituting $\omega = Kr\sin\theta$ into the expansion and inserting the resulting $g(Kr\sin\theta)$ into (1.31), we obtain

$$1 = K \int_{-\frac{\pi}{2}}^{\frac{\pi}{2}} \cos^2\theta \left[g(0) + \frac{1}{2} g''(0)(Kr)^2 \sin^2\theta + O(r^4) \right] d\theta \tag{1.37}$$

$$= K g(0) \underbrace{\int_{-\frac{\pi}{2}}^{\frac{\pi}{2}} \cos^2\theta \, d\theta}_{=\frac{\pi}{2}} + \frac{K g''(0)(Kr)^2}{2} \underbrace{\int_{-\frac{\pi}{2}}^{\frac{\pi}{2}} \cos^2\theta \sin^2\theta \, d\theta}_{=\frac{\pi}{8}} + O(r^4). \tag{1.38}$$

Hence, the self-consistency equation becomes

$$1 = \frac{\pi}{2} K g(0) + \frac{\pi}{16} K^3 g''(0) r^2 + O(r^4). \tag{1.39}$$

Using equation (1.7) and introducing the normalized distance above the threshold as follows

$$\mu = \frac{K - K_c}{K_c}, \tag{1.40}$$

equation (1.39) can be rewritten as

$$\mu = -\frac{\pi}{16} K_c^3 g''(0) r^2 + O(r^4). \tag{1.41}$$

Solving for r to leading order yields the square-root scaling law

$$r \approx \sqrt{\frac{16}{\pi K_c^3}} \sqrt{\frac{\mu}{-g''(0)}}. \tag{1.42}$$

This result shows that the bifurcation is *supercritical* when $g''(0) < 0$, whereas, if $g''(0) > 0$, the bifurcation becomes *subcritical*. This is exactly what Proposition 1.11 states.

Chapter 2

Adaptive Synchronization in Neural Systems

2.1 The Need for an Adaptive Model

The classical Kuramoto model, as discussed in the previous chapter, provides an elegant and powerful framework for understanding the transition from disorder to synchrony. However, when transitioning from the study of abstract oscillators to the investigation of neuronal populations in the brain, several fundamental assumptions of the original model must be re-evaluated. This makes the model *adaptive*, in the sense that both the natural frequencies $\omega_i(t)$ and the coupling strengths $K_{ij}(t)$ are allowed to evolve over time, so that the dynamics of the oscillators and the dynamics of the connections jointly determine the emergence of collective synchronization.

In biological neural networks, synchronization is not a static property but a highly dynamic and adaptive process. To bridge the gap between mathematical abstraction and neurobiological reality, we must address three primary limitations of the classical framework.

1. **Dynamic Coupling:** The classical assumption of a constant and uniform coupling strength K fails to capture the essence of synaptic transmission. Neural connections are subject to plasticity where the strength of an interaction evolves based on the activity of the synaptic neurons. Furthermore, synaptic efficacy is modulated by neurotransmitter depletion and external chemical signals, necessitating a time-dependent coupling matrix $K_{ij}(t)$.

2. **Non-Trivial Connectivity Architectures:** While the mean-field approximation assumes an all-to-all (fully connected) topology, the brain is organized into complex

and often sparse networks. The spatial arrangement of neurons plays a crucial role in determining how synchronization emerges and propagates.

3. **Intrinsic Frequency Variability:** In the standard model, natural frequencies ω_i are sampled from a stationary distribution $g(\omega)$ and remain constant throughout the evolution of the system. In contrast, biological neurons exhibit time-varying firing rates due to intrinsic homeostatic mechanisms (i.e., regulatory mechanisms that stabilize neuronal firing rates by adapting intrinsic excitability), changes in membrane excitability and neuromodulation. A realistic model must therefore account for non-stationary natural frequencies.

By relaxing these constraints, we move from a description of a physical system in equilibrium to a model of an adaptive information-processing system. In the following sections, we will formalize these generalizations, exploring how the interplay between time-varying parameters and specific network topologies gives rise to complex dynamical states, such as quasi-synchronization and intermittent coherence, which are characteristic of functional brain activity.

2.2 Formalization of the Generalized Model

To capture the complex interplay between the intrinsic dynamics of neurons and their adaptive interactions, we extend the classical Kuramoto governing equations. The generalization rests on the transition from static parameters to time-dependent functions, allowing the model to represent non-stationary biological processes.

In the brain, neurons communicate through a complex network of connections. The axon of a neuron transmits signals to other neurons through synapses, which connect to the dendrites of neighboring neurons. In these synapses, electrochemical neurotransmitters are released and can have either an excitatory or inhibitory effect on the receiving neuron. This interaction influences whether the neuron will generate an electrical impulse.

The natural frequency ω_i of each oscillator of the Kuramoto model can be interpreted as the intrinsic firing rate of a neuron. Since real neurons are not perfectly stationary systems, the internal state of a neuron can change over time. To take into account this feature, a more realistic formulation of the Kuramoto model can include time–dependent natural frequencies, denoted by $\omega_i(t)$.

Another aspect to consider is that, unlike in the classical model, real neuronal connections are heterogeneous and dynamic. Synaptic efficacy can change due to activity,

plasticity mechanisms, or variations in neurotransmitter release. For this reason, it is reasonable to introduce time–dependent and pair–dependent coupling strengths $K_{ij}(t)$.

Furthermore, the standard Kuramoto model assumes an all–to–all coupling structure, meaning that every oscillator interacts with every other one. However, neuronal networks exhibit complex connectivity patterns rather than uniform global coupling. Different neurons may be connected in specific configurations depending on anatomical and functional constraints.

These considerations lead to a generalized Kuramoto model suitable for describing neuronal synchronization.

Definition 2.1 (Generalized Neuronal Kuramoto Model)**.** *The dynamical evolution of a population of N coupled neurons is governed by the following system of non-autonomous ordinary differential equations:*

$$\dot{\theta}_i(t) = \omega_i(t) + \frac{1}{N}\sum_{j=1}^{N} K_{ij}(t)\sin\big(\theta_j(t) - \theta_i(t)\big), \quad i = 1, \dots, N, \tag{2.1}$$

where $\theta_i(t)$represents the phase of the i-th neuron, $\omega_i(t)$ is its time-varying natural frequency, and $K_{ij}(t)$ is the dynamic coupling strength between neuron j and neuron i.

Observation 2.2. *If both the natural frequencies $\omega_i(t)$ and the coupling strengths $K_{ij}(t)$ are time-independent, i.e.*

$$\omega_i(t) = \omega_i, \quad K_{ij}(t) = K_{ij},$$

then system (2.1) *reduces to the classical Kuramoto model* (1.4)*.*

Now, since the order parameter of the Kuramoto model has already been introduced in the classical framework, we recall it here in order to emphasize the different role it plays in the generalized model.

Definition 2.3 (Order parameter)**.** *Given the phases $\theta_1(t), \dots, \theta_N(t)$, the Kuramoto order parameter is defined as*

$$r(t)e^{i\psi(t)} = \frac{1}{N}\sum_{j=1}^{N} e^{i\theta_j(t)}, \tag{2.2}$$

where $r(t) \in [0, 1]$ measures the degree of phase coherence and $\psi(t)$ denotes the average phase of the system.

In the classical Kuramoto model, $r(t)$ is mainly used to detect the transition from incoherence to a stationary synchronized state as the coupling strength increases. In the present generalized framework, however, the presence of time-varying natural frequencies and coupling strengths prevents the system from reaching a stationary regime.

Consequently, $r(t)$ must be regarded as a genuinely time-dependent observable whose evolution reveals dynamical patterns of synchronization, such as intermittent synchronization, quasi-synchronization, and time-dependent coherence effects arising from the adaptive nature of the model.

Definition 2.4 (Time-varying coupling strength matrix)**.** *The coupling strength between neuron j and neuron i is described by the time-dependent matrix*

$$K_{ij}(t) = \gamma + \mu \sin\big(2\pi h_{ij} t + \psi_{ij}\big), \tag{2.3}$$

where γ denotes the mean coupling level, μ is the amplitude of the coupling variation, h_{ij} determines the rate at which the synaptic strength evolves in time, ψ_{ij} is a phase offset accounting for heterogeneity among different connections.

This formulation allows each synaptic connection to vary independently in time, modelling the adaptive nature of synaptic interactions such as plasticity and neurotransmitter dynamics. In particular, the parameters g_{ij} and ψ_{ij} introduce heterogeneity in both the temporal evolution and the phase of the coupling, which is a key feature in reproducing realistic neuronal connectivity patterns.

A second key generalization involves the intrinsic dynamics of each neuron. Unlike the classical Kuramoto oscillators, neurons do not exhibit strictly constant natural firing rates. Instead, their intrinsic frequencies may vary in time due to changes in membrane potential and threshold levels.

Definition 2.5 (Time-varying natural frequencies)**.** *The natural frequency of neuron i is assumed to be time-dependent and is defined as*

$$\omega_i(t) = \alpha_i + \beta_i \sin\big(2\pi f_i t + \phi_i\big), \tag{2.4}$$

where $\alpha_i, \beta_i \in \mathbb{R}$ and $f_i, \phi_i \in \mathbb{R}$ for all $i = 1, \ldots, N$. α_i represents the baseline frequency, while β_i and f_i define the amplitude and frequency of the internal modulation.

By combining the previous definitions, we obtain a model in which both the intrinsic dynamics of the neurons and the interactions among them evolve in time. This leads

to a fully time-dependent extension of the Kuramoto framework, specifically tailored to describe neuronal synchronization.

Under Definitions 2.4 and 2.5, the evolution of the phases is governed by

$$\dot{\theta}_i(t) = \alpha_i + \beta_i \sin\left(2\pi f_i t + \phi_i\right) + \frac{1}{N}\sum_{j=1}^{N}\left[\gamma + \mu \sin\left(2\pi h_{ij} t + \psi_{ij}\right)\right]\sin(\theta_j - \theta_i), \quad i = 1, \ldots, N. \tag{2.5}$$

2.3 Architectures of Neural Connectivity

In the brain, neurons are not organized in a random fashion, nor are they always globally connected. The spatial and functional organization of synaptic links—the network topology—defines the pathways through which synchronization signals propagate. In this section, we transition from the mean-field "all-to-all" assumption to more biologically plausible architectures. To mathematically represent these structures, we use the coupling matrix K_{ij} introduced in Equation (2.1). The presence or absence of a connection between neuron j and neuron i is defined by the topology of the underlying graph.

To illustrate how the structure of interactions influences the collective dynamics, we examine several standard connectivity patterns representing increasing levels of complexity in neural communication. We consider a simple system composed of four coupled oscillators. Despite its small size, this system already allows for different possible interaction architectures, depending on how the oscillators are connected to one another. The main configurations considered in this work are illustrated in Figure 2.1.

A key feature of the generalized model is the ability to define directed connections. In the brain, chemical synapses are inherently unidirectional: neuron i influences neuron j, but the reverse is not necessarily true unless a specific feedback synapse exists. Each configuration corresponds to a different connectivity matrix K, where x denotes a non-zero coupling strength. We now provide the explicit definition of these matrices related to the correspondent configuration.

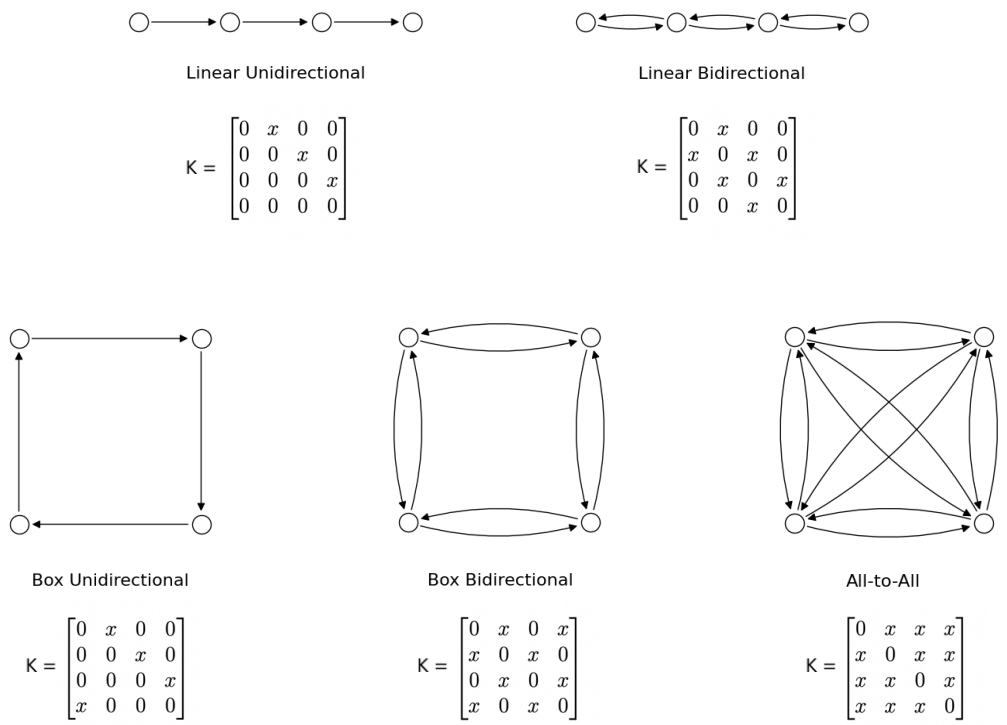

Figure 2.1: Schematic representation of different network communication architectures for a four-node system. Linear Unidirectional: a simple chain where information flows sequentially from the source to the terminal node; Linear Bidirectional: a chain-like structure featuring reciprocal exchange between adjacent nodes; Box Unidirectional: a single directed closed-loop; Box Bidirectional: a square lattice where adjacent nodes maintain mutual coupling; All-to-All (Fully Connected): a complete graph where every node is directly and bidirectionally linked to all others in the ensemble. Each arrow represents the direction of data flow or coupling between the units. The corresponding connectivity is mathematically defined by the matrix K.

2.4 Numerical Analysis of Adaptive Synchronization

We now investigate the behavior of the generalized Kuramoto model through numerical simulations. The aim is to analyze how different parameters affect the degree of synchronization in a population of oscillators and to discuss the implications of these results in the context of neuronal systems.

2.4.1 Effect of Static Coupling Strength

To investigate the role of coupling strength, we simulate the system for different values of K while keeping all other parameters fixed. For small values of K, the interaction between oscillators is weak and each oscillator evolves essentially according to its own natural frequency. As a consequence, the phases remain scattered and the order parameter remains close to zero. As the coupling strength increases, the interaction term becomes more influential and synchronization also increases.

Biologically, the sign of the coupling parameter K can be interpreted in terms of the nature of synaptic interactions.

- *excitatory synapses*: when $K > 0$ neurons tend to stimulate the activity of other neurons in the network. As a result, the firing of one neuron increases the likelihood that connected neurons will fire as well, promoting simultaneous activity and global synchronization.
- *inhibitory synapses:* in contrast, when $K < 0$, the activity of a neuron tends to suppress the firing of other neurons, reducing the probability of simultaneous spikes and leading to desynchronization of the network.

To evaluate the dynamics of the system, we perform numerical simulations using a population of $N = 1000$ coupled oscillators. The natural frequencies ω_i are sampled from a normal distribution $\mathcal{N}(\mu, \sigma^2) = \mathcal{N}(0, 0.5)$, and the evolution of the order parameter is computed over a time horizon of $T = 30$.

We begin by establishing a baseline comparison between excitatory and inhibitory static coupling. For these initial cases, we assume an all-to-all connectivity. In the Excitatory case ($K = 2.0$) the system is initialized in a completely disordered state, with phases θ_i uniformly distributed in $[0, 2\pi)$. For the Inhibitory case ($K = -2.0$) the system is initialized in a highly synchronized state, with phases concentrated around π according to a narrow normal distribution $\mathcal{N}(\pi, 0.1)$. As we can see in Figure 2.2, the excitatory coupling quickly drives the system from $r \approx 0$ to a state of nearly global synchronization. Conversely, the inhibitory coupling causes a rapid collapse of the initial synchronization, with the order parameter dropping toward zero and remaining in a state of incoherence.

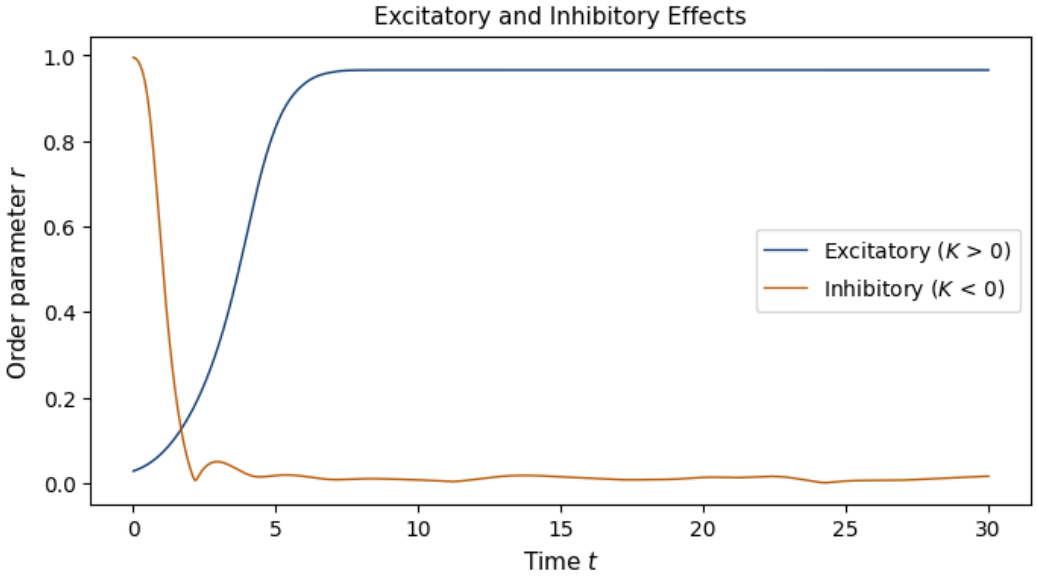

Figure 2.2: Evolution of the order parameter $r(t)$ for different static coupling regimes. The blue line represents excitatory coupling ($K = 2.0$), showing a rapid transition from a disordered state to global synchronization. The orange line illustrates the effect of inhibitory coupling ($K = -2.0$), where an initially synchronized population quickly collapses into an incoherent state.

The assumption of a uniform coupling strength K is, however, a strong idealization. A more realistic approach consists in allowing K to vary across neuronal pairs, decomposing the coupling matrix as

$$K_{ij} = \mu + \delta_{ij}, \tag{2.6}$$

where μ represents the mean coupling strength, defining the global baseline of interaction in the network. The terms δ_{ij} controls the amplitude of the system's fluctuations. In our modeling and simulations, these fluctuations are assumed to be independent and identically distributed random variables sampled from a Gaussian distribution $\delta_{ij} \sim \mathcal{N}(0, \sigma^2)$. By imposing a zero mean on the distribution of δ_{ij}, we ensure that μ remains the expected value of the coupling across the entire population, while the standard deviation σ directly controls the amplitude of the fluctuations and, consequently, the degree of structural disorder.

Substituting this into the model (2.1) yields

$$\dot{\theta}_i = \omega_i + \frac{\mu}{N} \sum_{j=1}^{N} \sin(\theta_j - \theta_i) + \frac{1}{N} \sum_{j=1}^{N} \delta_{ij} \sin(\theta_j - \theta_i). \tag{2.7}$$

Numerical evidence suggests that synchronization increases when the mean value of the coupling strengths is large and their variance is small. Conversely, large fluctuations in the coupling matrix tend to reduce global synchronization. While the mean coupling μ acts as the primary driver for synchronization, high standard deviation σ can introduce local instabilities or slightly delay the onset of a fully coherent state.

From a biological perspective, changes in the mean coupling strength μ have measurable consequences at the macroscopic level of brain activity. Large populations of neurons generate collective electric and magnetic fields, which give rise to the oscillatory patterns recorded through electroencephalography (EEG) and magnetoencephalography (MEG). When μ increases, neurons tend to oscillate in a more coordinated fashion, and this enhanced phase alignment results in an increase in the power of specific EEG/MEG frequency bands. Conversely, when synaptic interactions are weak or highly variable, the resulting desynchronization leads to low-amplitude, irregular oscillatory activity.

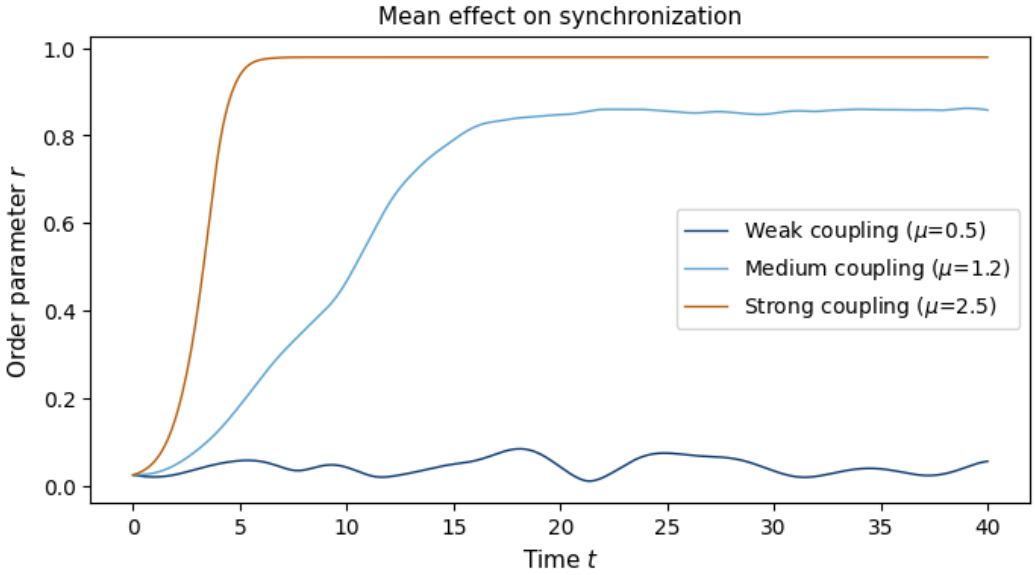

Figure 2.3: Impact of the mean coupling strength μ on the emergence of collective oscillations. The fluctuations are sampled for a Gaussian distribution $\delta_{ij} \sim \mathcal{N}(0, 0.01)$. For weak coupling ($\mu = 0.5$), the system remains in an incoherent state as the natural frequency dispersion ω_i dominates the dynamics. At a medium coupling level ($\mu = 1.2$), a phase transition begins, leading to partial synchronization. Strong coupling ($\mu = 2.5$) overcomes the individual frequency differences, driving the system toward a rapid and nearly complete synchronization.

These macroscopic signatures are clinically relevant. EEG analysis is routinely used to diagnose neurological conditions such as epilepsy, where pathological hypersynchro-

nization produces large-amplitude, highly coherent discharges, as well as sleep disorders and brain lesions, which alter the normal organization of oscillatory rhythms. In this sense, the model captures a fundamental mechanism: excessive coupling may push the system toward abnormally synchronized states, whereas strong fluctuations in synaptic efficacy tend to disrupt coherent neuronal activity.

To numerically validate these results, we transition to a model based on Equations (2.7) where the interaction strength between any two neurons is no longer constant but drawn from a distribution. This allows us to isolate two critical factors: the mean coupling strength μ, which represents the average synaptic efficacy, and the variance σ^2, which represents the "noise" within the network's connectivity. Simulations were performed using a population of $N = 1000$ oscillators over a time horizon of $T = 40$ for Figures 2.3, 2.5 and $T = 80$ for 2.4. The integration step is $dt = 0.1$.

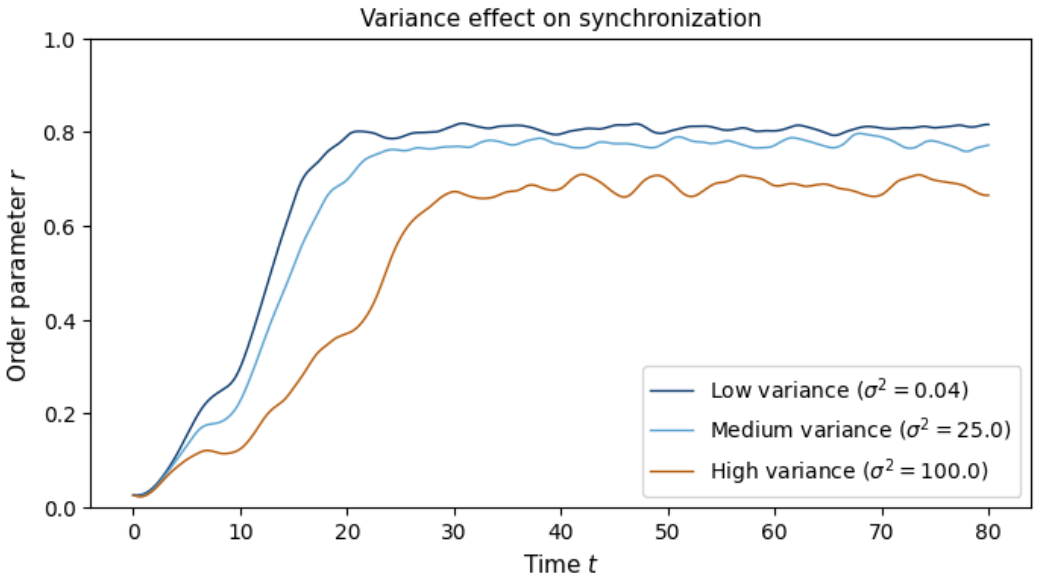

Figure 2.4: Impact of the variance on synchronization. The fluctuations are sampled from a Gaussian distribution $\delta_{ij} \sim \mathcal{N}(0, \sigma^2)$. The mean coupling strength is kept fixed at $\mu = 1.1$, while the variance is varied across $\sigma^2 = 0.04, 25.0, 100$. For small variance, the system synchronizes more easily, while large fluctuations progressively disrupt synchronization.

In the first scenario, we investigate the influence of the mean coupling μ while maintaining a low variance ($\sigma^2 = 0.01$). As illustrated in Figure 2.3, the system undergoes a clear transition: as the mean do increase, synchronization becomes stronger. In the second case, in Figure 2.4, we can see how, while a small variance ($\sigma^2 = 0.04$) allows the system to reach synchronization easily, a high variance ($\sigma^2 = 25.0$) gets the degree

of synchronization of the system worse. Finally, we evaluate the impact of connectivity noise by fixing the mean coupling at a high value ($\mu = 2.0$) and varying the standard deviation σ. As shown in Figure 2.5, despite the variance changes significantly ($\sigma^2 = 0.04$, $\sigma^2 = 4.0$, $\sigma^2 = 25.0$), the mean coupling μ keeps the synchronization level high. Namely, the mean coupling remains the primary driver of synchronization.

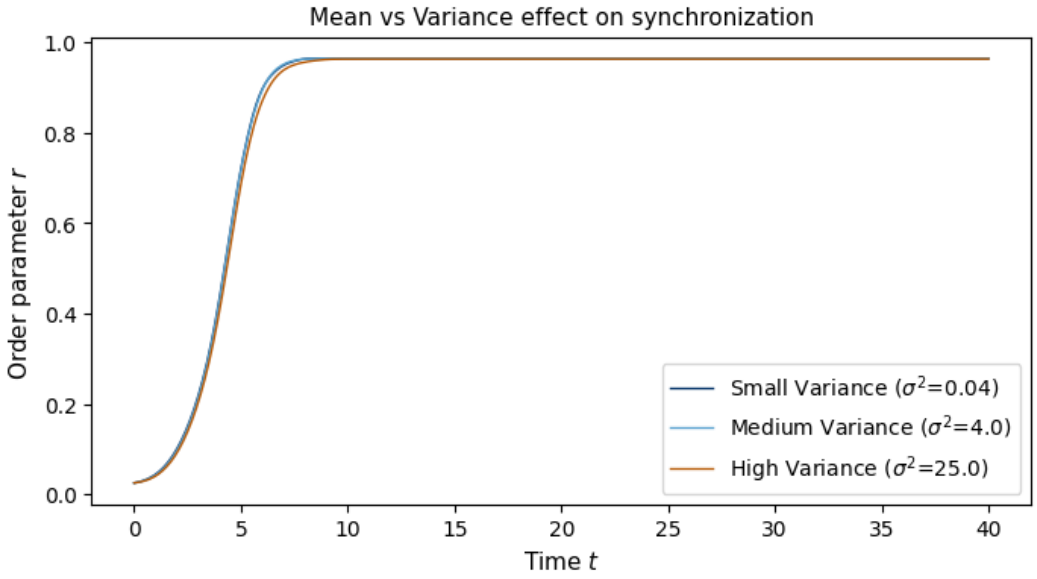

Figure 2.5: Robustness of synchronization against noise σ^2. With the mean coupling fixed at $\mu = 2.0$, the network is simulated under three levels of heterogeneity: small ($\sigma^2 = 0.04$), medium ($\sigma^2 = 4.0$), and high ($\sigma^2 = 25.0$) variance. The results demonstrate that while high variance can slightly delay the onset of coherence or introduce minor instabilities, the mean coupling μ remains the primary driver of synchronization. This highlights the resilience of neuronal populations to a certain degree of synaptic variability.

2.4.2 Effect of Dynamic Coupling Strength

To account for phenomena such as synaptic plasticity, neuromodulation, or slow fluctuations in synaptic efficacy, we introduce a time-dependent coupling matrix (2.3). Allowing the coupling strengths to vary in time enriches the dynamics of the system, giving rise to behaviors such as intermittent synchronization and the formation of transiently coherent clusters.

Definition 2.6 (Quasi-synchronization)**.** *We refer to* quasi-synchronization *as a dynamical regime in which the order parameter remains on average high, indicating a significant degree of phase coherence, but exhibits intermittent drops caused by temporal*

fluctuations in the coupling strengths. In this regime, the system repeatedly approaches and departs from a synchronized state without settling into either full coherence or complete incoherence.

Time–dependent coupling may lead to quasi-synchronization when interaction strengths fluctuate on time scales comparable to the intrinsic synchronization dynamics of the network. In realistic neuronal systems, synaptic interactions typically evolve much more slowly than the membrane and firing dynamics of individual neurons. For this reason, the modulation frequency h_{ij} governing the temporal variation of $K_{ij}(t)$ is expected to satisfy $h_{ij} \ll 1$, corresponding to slowly varying synaptic interactions.

Biologically, the speed at which the coupling varies dictates the functional state of the network:

- *Slowly varying coupling*: If the interaction changes slowly compared to the response time of the network, oscillators have sufficient time to adapt their phases to the instantaneous coupling structure. The system can reach and maintain a stable synchronized state, leading to sustained, coherent oscillations.
- *Rapidly varying coupling*: If the coupling strength fluctuates too rapidly, the oscillators cannot follow the evolving interaction structure. Consequently, global synchronization is lost or becomes highly unstable, resulting in fragmented or irregular oscillatory activity.

From a macroscopic perspective, this balance between time scales is crucial for the functional flexibility of the brain. When the effective coupling increases slowly, the enhanced phase alignment results in a gradual and sustained increase in EEG/MEG power within specific frequency bands. This is typically observed during processes such as sustained attention, slow neuromodulatory regulation, or transitions between sleep stages.

Clinically, these dynamic macroscopic signatures are just as relevant as static ones. While an overall excessive coupling may push the system toward epilepsy, an abnormally fast variation in synaptic efficacy can prevent coherent communication between brain areas, disrupting normal oscillatory rhythms. In this sense, the model illustrates a fundamental principle: static coupling defines the baseline potential for synchronization, whereas dynamic coupling provides the flexible, transient coordination required for complex cognitive tasks.

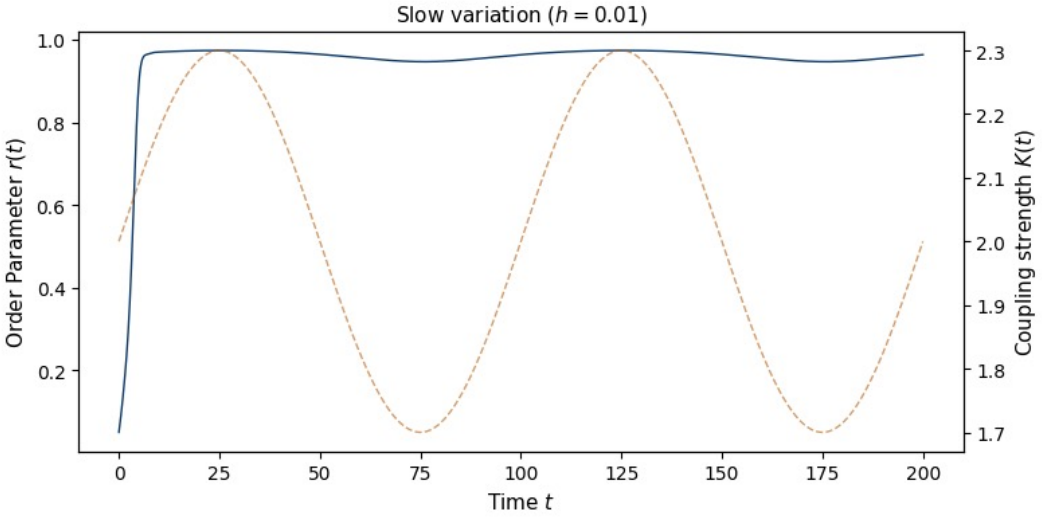
Slow variation ($h = 0.01$)
Order Parameter $r(t)$
Coupling strength $K(t)$
Time t
1.0
0.8
0.6
0.4
0.2
2.3
2.2
2.1
2.0
1.9
1.8
1.7
0
25
50
75
100
125
150
175
200

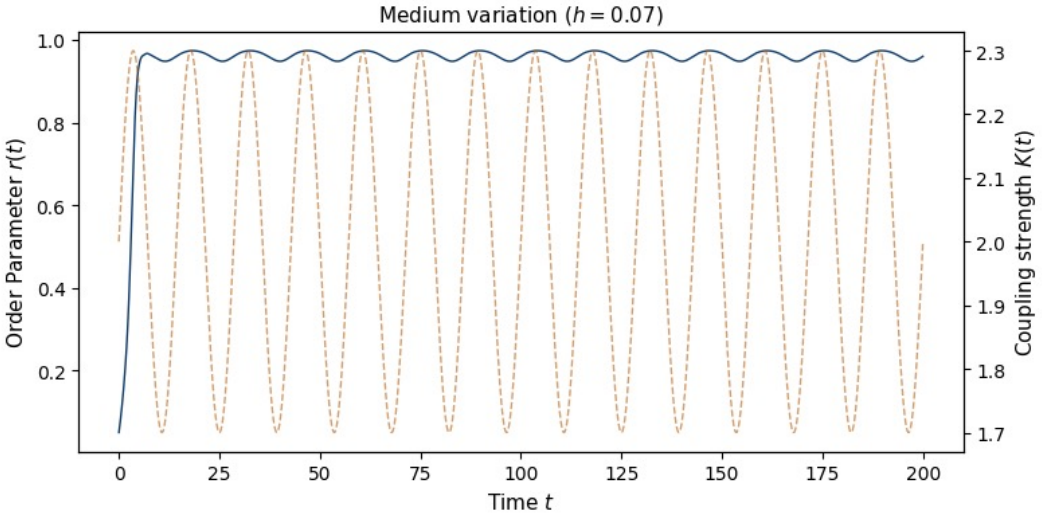
Medium variation ($h = 0.07$)
Order Parameter $r(t)$
Coupling strength $K(t)$
Time t
1.0
0.8
0.6
0.4
0.2
2.3
2.2
2.1
2.0
1.9
1.8
1.7
0
25
50
75
100
125
150
175
200

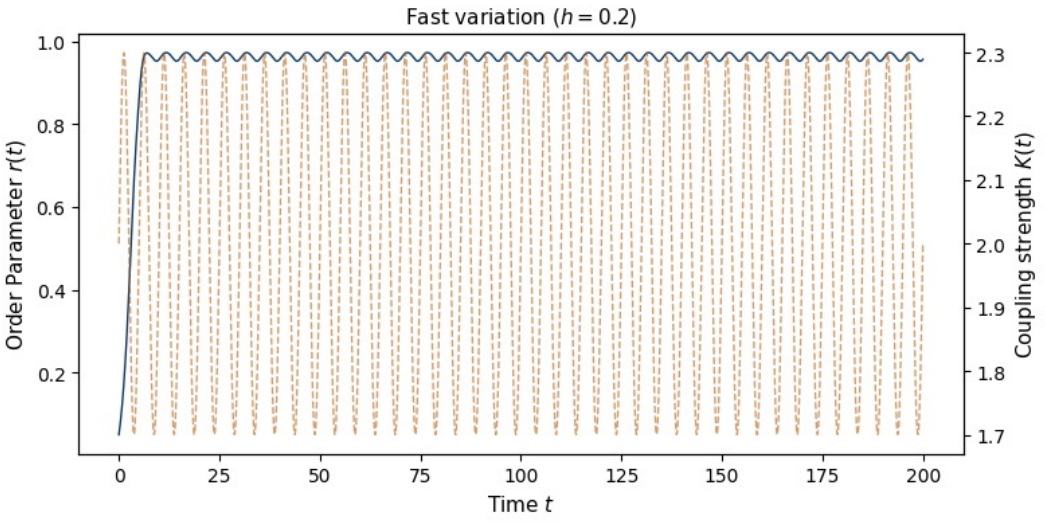

Figure 2.6: Effect of the modulation rate h on the dynamics of a Kuramoto network with time-varying coupling. Each panel shows the temporal evolution of the order parameter $r(t)$ (blue line) together with the corresponding coupling strength $K(t)$ (dashed line) for a network of $N = 500$ all-to-all coupled oscillators. In the first graphic slow variation is simulated ($h = 0.01$). The coupling changes sufficiently slowly for the network to adapt to its instantaneous value. The system remains fully synchronized, and $r(t)$ exhibits only mild oscillations that follow the slow modulation of $K(t)$. In the second figure medium variation ($h = 0.07$) is simulated. The modulation rate becomes comparable to the intrinsic relaxation time of the network. The system stays synchronized on average, but $r(t)$ displays more pronounced fluctuations, illustrating a regime of quasi-synchronization in which coherence is high yet dynamically modulated by the time-varying coupling. In the last figure, fast variation ($h = 0.2$) is plotted. The coupling fluctuates too rapidly for the oscillators to follow. The network effectively responds only to the mean value of $K(t)$, and the order parameter becomes nearly constant despite the rapid oscillations of the coupling strength.

To investigate how the temporal scale of synaptic modulation affects collective dynamics, we simulate a network of $N = 500$ Kuramoto oscillators with all-to-all connectivity. The natural frequencies ω_i are drawn from a Gaussian distribution with zero mean and standard deviation $\sigma = 0.5$, and the initial phases are sampled uniformly from $[0, 2\pi)$. The coupling strength varies in time according to Equation (2.3) with $\gamma = 2.0$ and $\mu = 0.3$, ensuring that the instantaneous coupling remains above the synchronization threshold. We compare three modulation frequencies h, corresponding to slow, intermediate, and fast temporal variation, in order to highlight the transition from adiabatic synchronization to quasi-synchronization and finally to an averaged-response regime.

2.4.3 Influence of Network Topology

Network structure can strongly affect synchronization dynamics by defining the pathways through which the coupling K_{ij} acts. In line with the architectures analyzed in Section 2.3, we observe that synchronization generally increases with the network's connectivity degree.

In the all-to-all configuration, every oscillator interacts with all others. As previously discussed for the mean coupling μ, this architecture promotes rapid synchronization because phase information propagates instantaneously across the entire population. In contrast, nearest-neighbor connectivity restricts interactions to local pairs. Here, global coherence develops more slowly, and the system often settles into local clusters: a regime where the effective coupling is strong locally but insufficient to bridge distant nodes.

From a biological perspective, these structural differences reflect the hierarchy of cortical connectivity. Highly connected "hub" regions facilitate the rapid propagation of phase information, supporting global oscillations captured by EEG and MEG. Conversely, localized or modular connectivity promotes the formation of functional clusters. This modular synchronization is a characteristic feature of cortical processing, allowing subsets of neurons to synchronize for specific tasks, such as sensory integration or working memory, while remaining functionally segregated from the rest of the network.

Random or irregular connectivity represents an intermediate regime. The density of these connections dictates the robustness of the collective dynamics: while dense networks stabilize coherent rhythms against fluctuations, sparse or fragmented networks are more susceptible to noise. Ultimately, the anatomical scaffold provides the necessary constraint within which the dynamic coupling $K_{ij}(t)$ must operate to achieve functional coordination.

In Figure 2.7 we simulated the Kuramoto model on the five distinct architectures previously described, exploring three different coupling regimes: weak ($K = 0.3$), intermediate ($K = 0.7$), and strong ($K = 1.1$). For all simulations, the natural frequencies ω_i are drawn from a normal distribution $\mathcal{N}(0, 0.04)$, and the system consisted of $N = 4$ oscillators. The dynamics are integrated over a total time $T = 200$ with a fixed time step $dt = 0.1$, using identical initial phases.

At the weakest coupling strength ($K = 0.3$), the impact of the underlying graph structure is most evident. The all-to-all configuration achieves the highest and fastest level of synchronization, reaching a steady-state order parameter $r(t) \approx 1.0$ almost instantaneously. Conversely, the unidirectional linear topology show the lowest coherence. A central observation in this regime is the impact of edge directionality: bidirectional

configurations consistently outperform unidirectional ones. This result suggests that reciprocal interactions between nodes promote phase locking more efficiently than a purely feedforward information flow. As the coupling strength increases to $K = 1.1$, the structural constraints imposed by the network become secondary to the interaction strength.

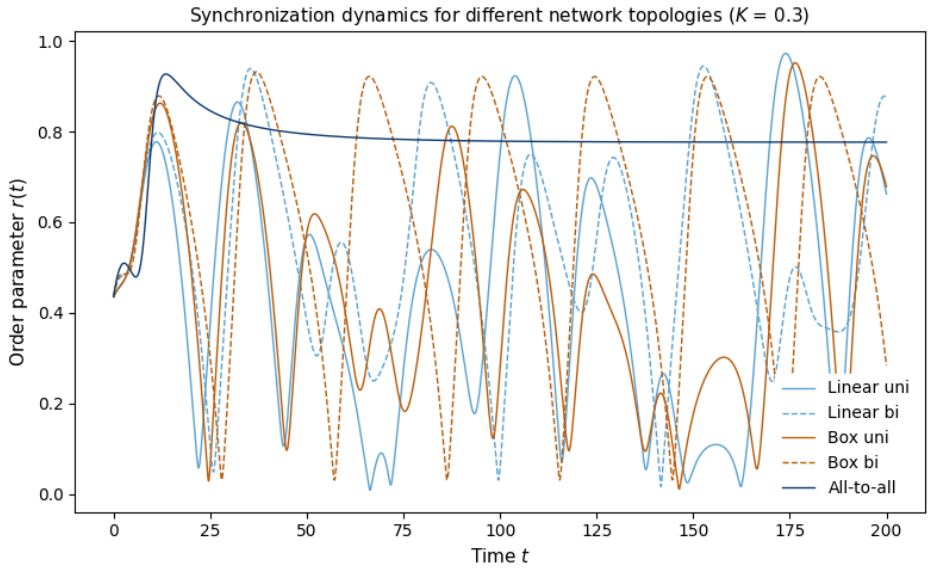

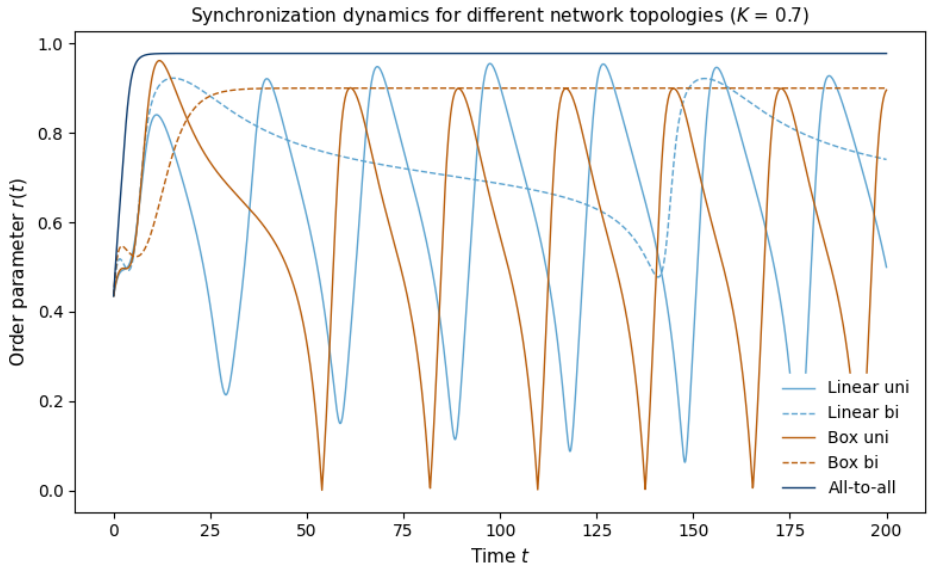

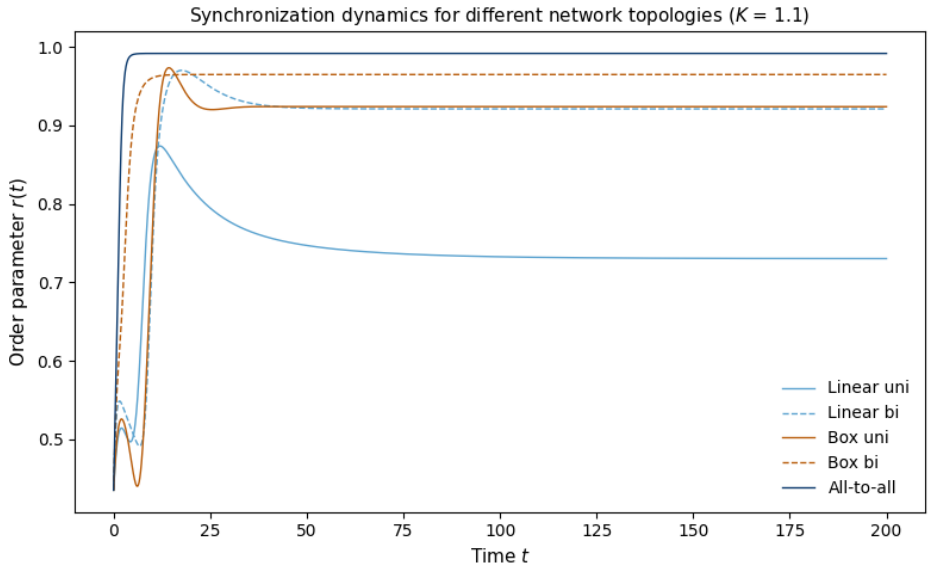

Figure 2.7: Evolution of the order parameter $r(t)$ over time for five different network topologies with $N = 4$ nodes. Each panel represents a different coupling strength: $K = 0.3$ (top), $K = 0.7$ (middle), and $K = 1.1$ (bottom). All simulations use the same initial phases, the same natural frequencies, and a fixed coupling strength. The comparison shows that denser and more symmetric networks synchronize more rapidly and reach higher coherence levels, while sparse or asymmetric architectures exhibit slower and less stable convergence. This illustrates the fundamental role of connectivity in shaping collective synchronization.

2.4.4 Static Frequency Distribution

The distribution of natural frequencies $g(\omega)$ is a fundamental determinant of the system's collective behavior. To better understand its impact, we first study the static case in which the natural frequencies ω_i are fixed in time, comparing a Gaussian and a Uniform distribution.

- *Gaussian Distribution*: Frequencies are drawn as $\omega_i \sim \mathcal{N}(\mu, \sigma^2)$. Numerical evidence shows that changing the mean μ does not affect the degree of synchronization, as it simply shifts the rotation of the entire population that depends on a phases difference. Instead the variance σ^2 is the critical parameter: as it increases, the frequencies become more dispersed, making it harder for the coupling K to align the phases, thus leading to a decrease in the order parameter r.

- *Uniform Distribution*: Frequencies are distributed in the interval $[-R, R]$ where $R \in \mathcal{R}$. Here, the synchronization threshold depends on the half-width R. As R increases, the intrinsic mismatch between oscillators grows, promoting desynchronization.

In the brain, neurons with similar intrinsic frequencies synchronize easily. A high degree of frequency dispersion ($\sigma^2 \gg 0$) prevents the formation of massive coherent discharges, which is essential for maintaining information processing and avoiding pathological hypersynchrony.

To illustrate these effects, we numerically simulate the Kuramoto model with all-to-all coupling and static natural frequencies. For both distributions (Gaussian and Uniform), we vary the parameter controlling frequency dispersion and take into account the evolution of the order parameter $r(t)$.

For all simulations in Figures 2.8 and 2.9, we use a population of $N = 500$ oscillators with all-to-all coupling. The coupling strength is fixed at $K = 1.5$, and the dynamics are integrated over a time window of $T = 40$ with a time step $dt = 0.05$. Natural frequencies are sampled either from a Gaussian distribution with variance $\sigma^2 \in \{0.04, 0.25, 1.00\}$ or from a Uniform distribution over $[-R, R]$ with $R \in \{0.5, 1.0, 2.0\}$. All simulations started from random initial phases.

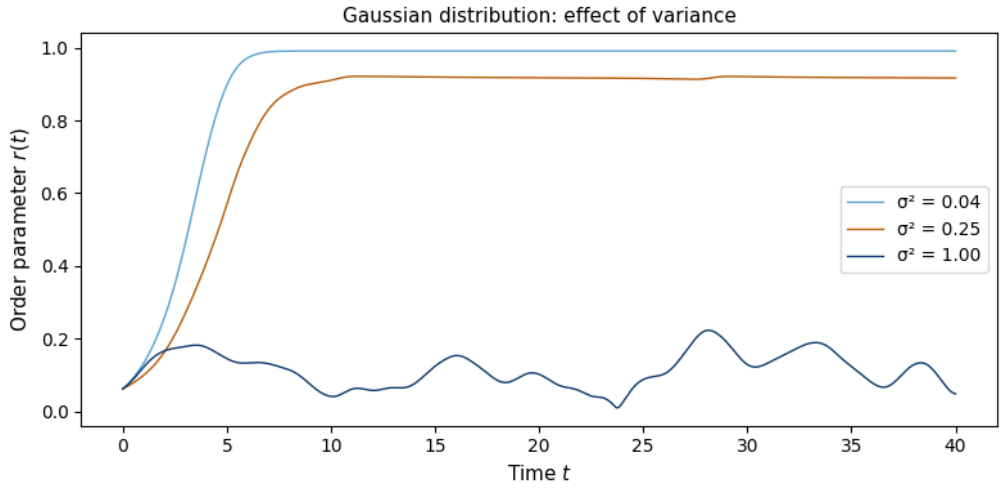

Figure 2.8: Temporal evolution of the order parameter $r(t)$ for a Gaussian frequency distribution $\mathcal{N}(\mu, \sigma^2)$. The plot illustrates how variance affects system synchronization: as it increases, the synchronization becomes lower.

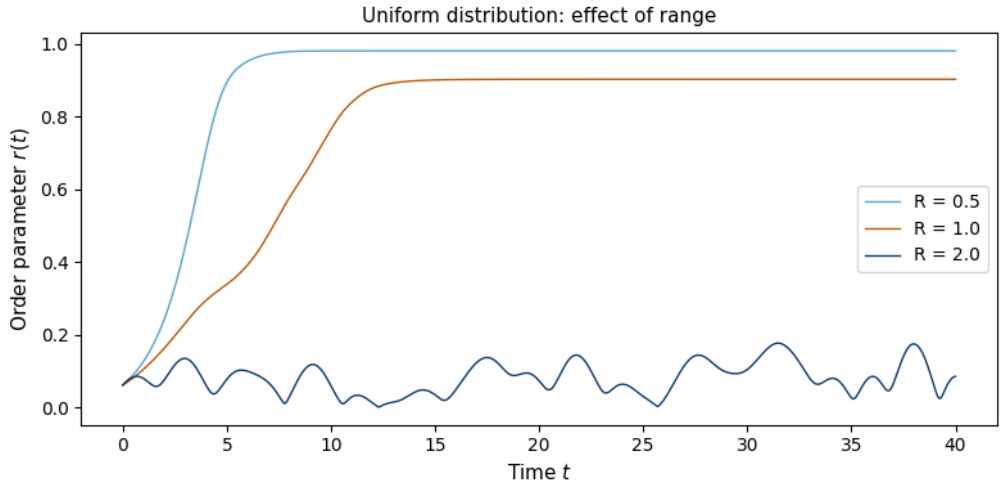

Figure 2.9: Influence of the frequency range R on collective synchronization in a Uniform distribution. The system's coherence is evaluated for frequencies distributed in the interval $[-R, R]$. A narrow range facilitates rapid convergence toward global synchronization. Conversely, widening the range to $R = 2.0$ increases the mismatch between oscillators, leading to a breakdown of global order.

2.4.5 Time-Dependent Natural Frequencies

A more complex scenario arises when the natural frequencies vary in time, $\omega_i(t)$. In this regime, the system's ability to synchronize depends on the rate of change of the intrinsic rhythms:

- *Slowly varying frequencies*: If the $\omega_i(t)$ change slowly, the system can "track" the variations. This leads to a regime of quasi-synchronization, where the network maintains a high level of coherence despite the shifting frequencies.
- *Fast varying frequencies*: When frequencies fluctuate rapidly, the oscillators cannot adapt their phases quickly enough. The system exhibits a more irregular synchronization, where $r(t)$ oscillates rapidly as units continuously enter and leave the synchronized cluster.

From a biological point of view, neurons with time-varying frequencies represent an adaptive network. Even with a small coupling K, if the frequencies evolve in a coordinated manner, the system can achieve synchronization. This mechanism allows the brain to enter and exit different "quasi-synchronous" states, supporting the transient formation of functional assemblies.

To validate these theoretical observations, we perform a numerical simulation of a Kuramoto model consisting of $N = 500$ all-to-all coupled oscillators. The system

is initialized with phases θ_i drawn from a uniform distribution in $[0, 2\pi)$, while the base natural frequencies follow a normal distribution $\mathcal{N}(0, 0.5)$. We keep the coupling strength constant at $K = 2.5$ to ensure the system operates above the synchronization threshold. We compare two distinct regimes: a slow modulation, where frequencies evolve according to a low-frequency sine wave, and a fast modulation, characterized by rapid oscillations. The evolution of the global coherence is monitored through the order parameter $r(t)$.

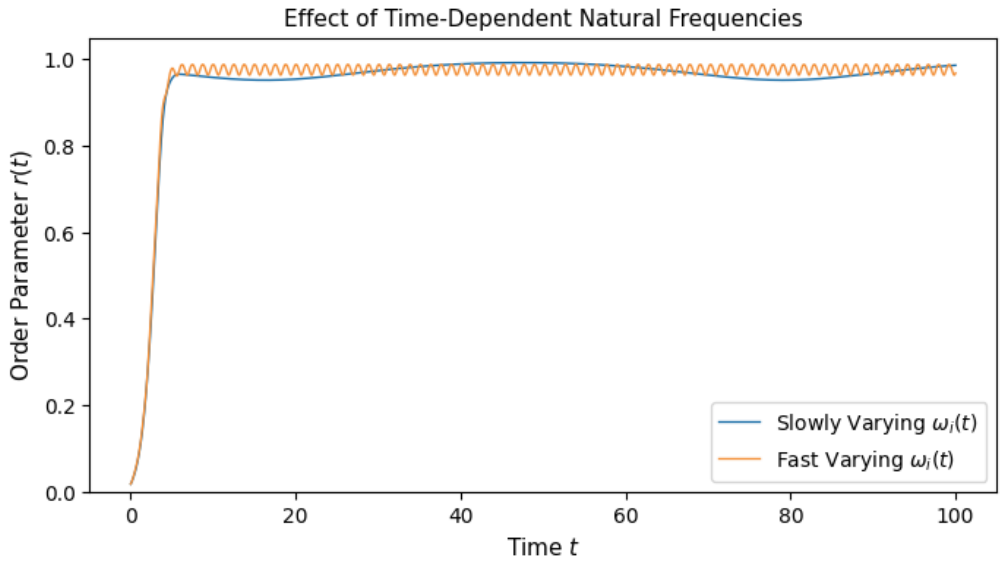

Figure 2.10: Evolution of the order parameter $r(t)$ under time-dependent natural frequencies. The plot compares the synchronization stability for $N = 500$ oscillators in two regimes: slowly varying frequencies (blue line, $\omega_i(t) \propto \sin(0.1t)$) and fast varying frequencies (orange line, $\omega_i(t) \propto \sin(5.0t)$). In the slow regime, the system effectively "tracks" the frequency shifts, maintaining a smooth quasi-synchronous state. Conversely, the fast regime exhibits rapid, high-frequency fluctuations in $r(t)$, reflecting the continuous attempts of the oscillators to re-synchronize as their intrinsic rhythms shift faster than the network's adaptation time.

2.4.6 Combined Effects on Synchronization

The emergence of synchronization in adaptive neural networks results from the interplay between multiple factors: the average coupling strength μ and its fluctuations δ_{ij}, the temporal modulation of the coupling matrix $K_{ij}(t)$ introduced in (2.3), the network topology described in Section 2.3, and the variability of the natural frequencies ω_i. Numerical simulations show that these elements do not act independently, but interact in nontrivial ways to shape the collective dynamics.

Strong and slowly varying coupling promotes global synchronization, particularly in densely connected networks where information about phase differences propagates efficiently. However, even in such favorable conditions, excessive heterogeneity in the natural frequencies may prevent full coherence, leading instead to partial or clustered synchronization. Conversely, in sparsely connected or locally structured networks, synchronization may remain confined to subsets of oscillators unless the effective coupling is sufficiently strong to compensate for the limited connectivity.

Dynamic coupling introduces an additional layer of complexity. Depending on the speed or frequency of these variations, the system can enter a state of quasi-synchronization, where high overall coherence is periodically interrupted by momentary drops in and out of synchronous behavior. When the coupling strength varies too rapidly, the oscillators have insufficient time to react and adapt to the changing network conditions, causing the system to lose its stable rhythm more frequently.

From a biological perspective, these combined effects reflect the multifaceted nature of neuronal synchronization. Coherent brain rhythms arise from the balance between synaptic strength, anatomical connectivity, intrinsic neuronal properties, and slow modulatory processes such as plasticity and neuromodulation. Disruptions in any of these components, such as reduced connectivity, abnormal synaptic variability, or excessive heterogeneity in intrinsic firing rates, can impair the emergence of coherent oscillations, as observed in various neurological disorders.

To validate theoretical results, the following simulation (Figure 2.11) investigate the evolution of synchronization in the Kuramoto model on a fully connected network consisting of $N = 500$ oscillators. The system is integrated up to a final time $T = 300$ with a time step $dt = 0.05$. The natural frequencies are initially drawn from a normal distribution $\mathcal{N}(0, 0.5)$, while the initial phases are uniformly distributed in the interval $[0, 2\pi]$. The aim is to analyze the combined effect of time-dependent variations in the coupling strength K and in the natural frequencies ω. To this end, four different scenarios are considered: constant K and constant ω; time-dependent $K(t)$ and constant ω; constant K and time-dependent; both $K(t)$ and $\omega(t)$ varying in time.

The results show that the fully static case tends toward a relatively stable synchronized state, whereas introducing temporal variability in the parameters leads to persistent fluctuations in $r(t)$. In particular, variations in the coupling strength $K(t)$ directly modulate the level of synchronization, while time-dependent natural frequencies $\omega(t)$ introduce a distributed perturbation that can hinder or modulate phase coherence.

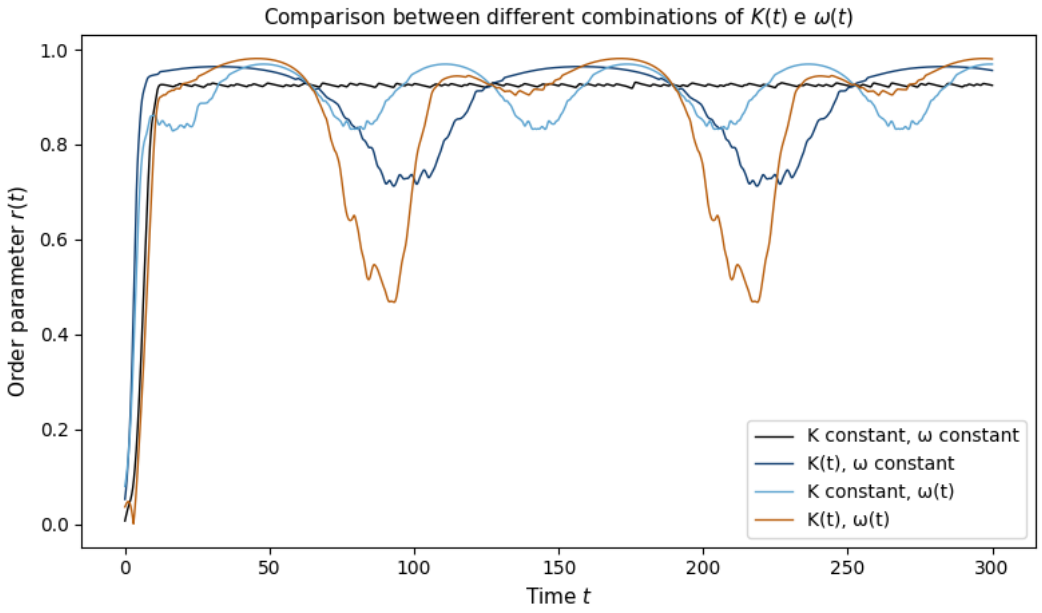

Figure 2.11: Time evolution of the order parameter $r(t)$ in the Kuramoto model on a fully connected network with $N = 500$ oscillators. Four scenarios are compared: constant coupling and constant natural frequencies (black), time-dependent coupling $K(t)$ with constant frequencies (dark blue), constant coupling with time-dependent frequencies $\omega(t)$ (light blue), and both $K(t)$ and $\omega(t)$ varying in time (orange). Temporal variability in the parameters induces fluctuations in the level of synchronization; in particular, variations in $K(t)$ have a direct impact on the strength of global synchronization.

Conclusions

The phenomenon of synchronization is a fundamental mechanism underlying the complex dynamics of the brain, enabling communication and information processing across distributed neural networks. In this thesis, we have explored the Kuramoto model as a powerful theoretical paradigm to understand how coherent collective behavior emerges from the interaction of individual oscillatory units.

We analyzed the classical Kuramoto model, providing a rigorous mathematical foundation for the transition from an incoherent state to macroscopic synchronization. Through the mean-field approximation and the analysis of the self-consistency equation, we analytically derived the critical coupling threshold K_c and characterized the bifurcation scaling. The theoretical predictions were validated through numerical simulations, confirming the phase transition for a population of oscillators with a Lorentzian frequency distribution.

However, what happens in the brain is far from a uniform and static system. In the second chapter, we consider a more general Kuramoto framework, relaxing some standard assumptions and exploring extensions such as complex networks, time-varying frequencies, and dynamic couplings through simulations.

Our numerical investigation of this adaptive model highlighted several key phenomena:

- **The Role of Connectivity:** The underlying network architecture strictly dictates the synchronization pathways. We observed that denser and bidirectional topologies (such as all-to-all or bidirectional boxes) facilitate rapid and robust phase-locking, whereas sparse or unidirectional architectures struggle to achieve global coherence, often settling into localized synchronous clusters.
- **Static vs. Dynamic Coupling:** While a strong, uniform mean coupling promotes global synchronization, the introduction of synaptic noise (variance) and inhibitory interactions can rapidly disrupt coherence. Furthermore, time-varying coupling uncovers the regime of *quasi-synchronization*. If the synaptic modulation is sufficiently slow, the network can smoothly track the interaction changes;

conversely, rapid fluctuations prevent the oscillators from adapting, leading to fragmented oscillatory activity.

- **Intrinsic Frequency Variability:** The dispersion of natural frequencies acts as a natural barrier against hypersynchronization. Moreover, allowing frequencies to evolve in time revealed that neural populations can enter and exit transient synchronous states, a mechanism that is crucial for dynamic cognitive tasks and functional flexibility.

Pathological states such as epilepsy can be viewed as an over-coupling that overcomes intrinsic heterogeneities, whereas cognitive flexibility relies on the brain's ability to maintain a controlled, intermediate level of coherence. The generalized Kuramoto model proves to be a highly versatile tool in this context, providing a macroscopic window into the microscopic complexities of neuronal dynamics, and offering a robust starting point for future investigations into network-driven brain disorders and adaptive learning rules.

Appendix A

Python Codes

This appendix provides the complete Python codes used to generate the numerical results presented in the main text. All the simulations were implemented in Python by using NumPy and Matplotlib libraries.

To begin with, the following functions implement the fundamental operations of the Kuramoto model simulations used to create Figure 1.2.

```
import numpy as np
import matplotlib.pyplot as plt

"""
First of all, we need a function that requires an integer N
which represents the number of oscillators and a
float gamma, namely the distribution width parameter.
The function returns the value omega, an array of N natural
frequencies sampled from a Lorentzian distribution.
"""

def lorentzian(N, gamma):
    return gamma * np.tan(np.pi * (np.random.rand(N) - 0.5))

"""
Then we define the following function. It requires an
array of the oscillators phases and returns a float number, the
order parameter, namely the absolute value of the complex mean.
"""
```

```python
def order_parameter(theta):
    return np.abs(np.mean(np.exp(1j * theta)))

"""
The next function we need performs an integration step. It requires:
- theta, an array containing the oscillators phases;
- omega, an array with the natural frequencies of oscillators;
- K, a float value, namely the coupling strength;
- dt, another float value which represents the time step.
The function returns a new array theta containing the updated
phases of the oscillators.
"""

def kuramoto_step(theta, omega, K, dt):

    r = order_parameter(theta)
    psi = np.angle(np.mean(np.exp(1j * theta)))

    theta_dot = omega + K * r * np.sin(psi - theta)
    return theta + dt * theta_dot

"""
The following function manages the entire simulation for a
specific coupling value K. It requires:
- N, an integer representing the number of oscillators;
- K, a float value, namely the coupling strength;
- gamma, a float for the Lorentzian distribution width;
- T, a float (default=60) for the total simulation time;
- dt, a float (default=0.1) for the integration time step;
- transient, a float (default=40) for the initial time
period to discard.
The function returns a float representing the average order
parameter r calculated after the system has reached
a stationary state.
"""

def simulate_kuramoto(N, K, gamma, T=60, dt=0.1, transient=40):

```

```
    omega = lorentzian(N, gamma)
    theta = np.random.uniform(0, 2*np.pi, N)
    steps = int(T / dt)
    transient_steps = int(transient/dt)
    r_vals = []

    for t in range(steps):
      z = np.mean(np.exp(1j * theta))
      r = np.abs(z)
      psi = np.angle(z)
      theta = kuramoto_step(theta, omega, K, dt)
      if t >= transient_steps:
        r_vals.append(r)

    return np.mean(r_vals)

"""
The following function manages the visual representation of the
synchronization transition. It requires:
- N, an integer representing the number of oscillators;
- gamma, a float for the Lorentzian distribution width;
- K_range, an array of float values for the coupling strength;
- n_runs, an integer (default=5) specifying the number of
  simulations to average for each K.
The function calculates the numerical order parameter, compares
it with the theoretical prediction and
displays the resulting bifurcation plot.
"""

def plot_bifurcation(N, gamma, K_range, n_runs=5):
    r_final_means = []

    for K in K_range:
      run_results = [simulate_kuramoto(N, K, gamma) for _ in range(n_runs)]
      r_final_means.append(np.mean(run_results))

    K_c = 2 * gamma
    K_theory = np.linspace(K_range.min(), K_range.max(), 500)
```

```
96
97      r_theory = np.zeros_like(K_theory)
98      mask = K_theory > K_c
99      r_theory[mask] = np.sqrt(1 - K_c / K_theory[mask])
100
101     plt.figure(figsize=(8, 6), facecolor='white')
102     plt.plot(K_range, r_final_means, 'o', color='black', markersize=3,
        ↪  label=f'Simulation (N={N})')
103     plt.plot(K_theory, r_theory, '--', color='black', linewidth=1,
        ↪  label=r'Theory')
104     plt.axvline(K_c, color='gray', linestyle='--', linewidth=1, label=r'$K_c
        ↪  = 2\gamma = ' + f'{K_c:.1f}$')
105
106     plt.xlabel(r"Coupling strength $K$", fontsize=11)
107     plt.ylabel(r"Order parameter $r$", fontsize=11)
108     plt.title("Transition of synchronization", fontsize=11)
109
110     plt.legend(fontsize=10, frameon=False)
111     plt.ylim(-0.02, 1.05)
112     plt.xlim(K_range.min(), K_range.max())
113
114     plt.tight_layout()
115     plt.show()
116
117 """
118 To generate the bifurcation diagram were used these parameters:
119 """
120
121 gamma_val = 1.0
122 K_vals = np.linspace(0, 5, 60)
123 plot_bifurcation(N=10000, gamma=gamma_val, K_range=K_vals, n_runs=20)
```

Then, to generate the results presented in Chapter 2, we switched to a dynamical model. The functions used for this new model are reported below. For the order parameter, we employed the same function previously defined.

```
1 """
2 The next function computes an integration step for the Kuramoto model
3 using the Euler method. It accounts for a time-varying coupling matrix
```

```
and provides the updated phases. It requires:
- theta: an array of current oscillator phases;
- omega_func: a function that returns the natural frequencies
  of the oscillators at time t;
- K_mat: a matrix representing the coupling strengths
  between each pair of oscillators;
- t: the current time;
- dt: the integration time step.
The function returns an array containing the updated phases of the
↪  oscillators.
"""

def kuramoto_dynamic_step(theta, omega_func, K_mat, t, dt):
    N = len(theta)
    diff = theta[np.newaxis, :] - theta[:, np.newaxis]
    coupling = np.sum(K_mat * np.sin(diff), axis=1) / N
    theta_dot = omega_func(t) + coupling
    return theta + dt * theta_dot

"""
The following function manages the entire temporal evolution of the system.
It iterates through the time steps, updating the phases and recording
the synchronization level at each point. It requires:
- theta0: an array of initial phases;
- omega_func: a function defining the natural frequencies;
- A: the adjacency matrix defining the network topology;
- K_func: it determines the coupling strength at each time step;
- T: the total simulation time (default=200);
- dt: the integration time step (default=0.1).
The function returns two arrays: one representing the time points and
one containing the evolution of the order parameter r.
"""

def simulate_kuramoto_dynamic(theta0, omega_func, A, K_func, T=200, dt=0.1):
    N = len(theta0)
    theta = theta0.copy()
    steps = int(T/dt)
    r_vals = np.zeros(steps)
```

```
    time = np.linspace(0, T, steps)

    for i, t in enumerate(time):
        r_vals[i] = order_parameter(theta)
        K_mat = K_func(t) * A
        theta = kuramoto_dynamic_step(theta, omega_func, K_mat, t, dt)

    return time, r_vals

"""
The following function computes a single integration step for the Kuramoto
model with heterogeneous coupling, according to
the decomposition (2.6). It requires:
- theta: an array of current oscillator phases;
- omega: an array of natural frequencies;
- mu: a float representing the mean coupling strength;
- delta_mat: a NxN matrix representing the fluctuations around the mean;
- dt: the integration time step.
The function calculates the mean interaction term and the fluctuation-driven
term separately to update the phase of each oscillator.
"""

def kuramoto_random_coupling_step(theta, omega, mu, delta_mat, dt):
    N = len(theta)
    diff = theta[np.newaxis, :] - theta[:, np.newaxis]
    sin_diff = np.sin(diff)

    mean_term = mu * np.sum(sin_diff, axis=1) / N
    fluct_term = np.sum(delta_mat * sin_diff, axis=1) / N

    theta_dot = omega + mean_term + fluct_term
    return theta + dt * theta_dot

"""
This function manages the numerical simulation of a network with random
coupling strengths to isolate the roles of average connectivity and
synaptic noise. It requires:
- N: an integer representing the number of oscillators;
```

```
- mu: a float for the mean coupling strength;
- sigma: a float representing the standard deviation of the
  coupling fluctuations;
- T: a float for the total simulation time (default=200);
- dt: a float for the integration time step (default=0.1).
The function initializes the system with random phases and natural
frequencies. It then generates the fluctuation matrix and returns
the evolution of the order parameter r(t).
"""

def simulate_random_coupling_kuramoto(N, mu, sigma, T=200, dt=0.1):
    np.random.seed(42)
    theta = np.random.uniform(0, 2*np.pi, N)
    omega = np.random.normal(0, 0.5, N)
    delta_mat = np.random.normal(0, sigma, (N, N))

    steps = int(T/dt)
    r_vals = np.zeros(steps)

    for i in range(steps):
        r_vals[i] = order_parameter(theta)
        theta = kuramoto_random_coupling_step(theta, omega, mu, delta_mat,
        ↪  dt)
    return r_vals
```

To generate Figure 2.2 we used the following code.

```
"""
These parameters and configurations were used:
- N = 1000: number of coupled oscillators;
- Natural frequencies: sampled from a normal distribution
- Connectivity: an all-to-all adjacency matrix ;
- Initial conditions: uniform distribution for excitatory cases and
  narrow normal distribution for inhibitory cases.
These simulations allow for the analysis of the system's response to
different coupling strengths and variance levels.
"""

N = 1000
```

```
np.random.seed(42)
omega_vals = np.random.normal(0, 0.5, N)

def omega_func_static(t):
    return omega_vals

A_all = np.ones((N, N)) - np.eye(N)

theta0_random = np.random.uniform(0, 2*np.pi, N)
K_exc = lambda t: 2.0
time_exc, r_exc = simulate_kuramoto_dynamic(theta0_random, omega_func_static,
↪  A_all, K_exc, T=30, dt=0.05)

theta0_synchronized = np.random.normal(np.pi, 0.1, N)
K_inh = lambda t: -2.0
time_inh, r_inh = simulate_kuramoto_dynamic(theta0_synchronized,
↪  omega_func_static, A_all, K_inh, T=30, dt=0.05)

plt.figure(figsize=(8, 4))
plt.style.use('default')
plt.plot(time_exc, r_exc, label='Excitatory ($K$ > 0)', color="#0D3B6E",
↪  linewidth=1)
plt.plot(time_inh, r_inh, label='Inhibitory ($K$ < 0)', color="#B85C0A",
↪  linewidth=1)
plt.title('Excitatory and Inhibitory Effects', fontsize = 11)
plt.xlabel('Time $t$', fontsize = 11)
plt.ylabel('Order parameter $r$', fontsize = 11)
plt.legend(loc='best', fontsize = 10)
plt.show()
```

To generate Figures 2.3, 2.4 and 2.5 we run the following codes.

```
N = 1000
T = 40
dt = 0.1
time = np.linspace(0, T, int(T/dt))
"""
To generate the "Mean Effect" Figure:
"""
```

```
8
9  plt.figure(figsize=(8, 4))
10 plt.style.use('default')
11
12 r_mu_05 = simulate_random_coupling_kuramoto(N, mu=0.5, sigma=0.1, T=T, dt=dt)
13 r_mu_12 = simulate_random_coupling_kuramoto(N, mu=1.2, sigma=0.1, T=T, dt=dt)
14 r_mu_25 = simulate_random_coupling_kuramoto(N, mu=2.5, sigma=0.1, T=T, dt=dt)
15
16 plt.plot(time, r_mu_05, label = r'Weak coupling ($\mu$=0.5)', color =
   ↪  "#0D3B6E", linewidth = 1)
17 plt.plot(time, r_mu_12, label = r'Medium coupling ($\mu$=1.2)', color =
   ↪  "#5BA3D0", linewidth = 1)
18 plt.plot(time, r_mu_25, label = r'Strong coupling ($\mu$=2.5)', color =
   ↪  "#B85C0A", linewidth = 1)
19 plt.title('Mean effect on synchronization', fontsize=11)
20 plt.xlabel('Time $t$', fontsize = 11)
21 plt.ylabel('Order parameter $r$', fontsize = 11)
22 plt.legend(loc='best',fontsize = 10)
23 plt.show()
24
25 """
26 To generate the "Variance Effect" Figure:
27 """
28
29 T_long = 80
30 time_long = np.linspace(0, T_long, int(T_long/dt))
31
32 plt.figure(figsize=(8, 4))
33 plt.style.use('default')
34
35 r_sig_small = simulate_random_coupling_kuramoto(N, mu=1.1, sigma=0.1,
   ↪  T=T_long, dt=dt)
36 r_sig_medium = simulate_random_coupling_kuramoto(N, mu=1.1, sigma=5.0,
   ↪  T=T_long, dt=dt)
37 r_sig_large = simulate_random_coupling_kuramoto(N, mu=1.1, sigma=10.0,
   ↪  T=T_long, dt=dt)
38
```

```
plt.plot(time_long, r_sig_small, label=r'Low variance ($\sigma^2=0.04$)', color="#0D3B6E", linewidth=1)
plt.plot(time_long, r_sig_medium, label=r'Medium variance ($\sigma^2=25.0$)', color="#5BA3D0", linewidth=1)
plt.plot(time_long, r_sig_large, label=r'High variance ($\sigma^2=100.0$)', color="#B85C0A", linewidth=1)

plt.title('Variance effect on synchronization', fontsize=11)
plt.xlabel('Time $t$', fontsize=11)
plt.ylabel('Order parameter $r$', fontsize=11)
plt.legend(loc='best', fontsize=10)
plt.ylim(0, 1)
plt.show()

"""
To generate the "Mean vs Variance Effect" Figure:
"""

r_sig_02 = simulate_random_coupling_kuramoto(N, mu=2.0, sigma=0.2, T=T, dt=dt)
r_sig_20 = simulate_random_coupling_kuramoto(N, mu=2.0, sigma=2.0, T=T, dt=dt)
r_sig_50 = simulate_random_coupling_kuramoto(N, mu=2.0, sigma=5.0, T=T, dt=dt)

plt.figure(figsize=(8, 4))
plt.style.use('default')
plt.plot(time, r_sig_02, label = r'Small Variance ($\sigma^2$=0.04)', color = "#0D3B6E", linewidth = 1)
plt.plot(time, r_sig_20, label = r'Medium Variance ($\sigma^2$=4.0)', color = "#5BA3D0", linewidth = 1)
plt.plot(time, r_sig_50, label = r'High Variance ($\sigma^2$=25.0)', color = "#B85C0A", linewidth = 1)
plt.title('Mean vs Variance effect on synchronization', fontsize = 11)
plt.xlabel('Time $t$', fontsize = 11)
plt.ylabel('Order parameter $r$', fontsize = 11)
plt.legend(fontsize = 10)
plt.show()
```

To generate Figure 2.6 we run the code below.

```
N, T, dt = 500, 100, 0.1
np.random.seed(42)
theta0 = np.random.uniform(0, 2*np.pi, N)
omega_const = np.random.normal(0, 0.5, N)
A_all_to_all = np.ones((N, N)) - np.eye(N)

omega_f = lambda t: omega_const
K_f = lambda t, h: 2.0 + 0.3* np.sin(2*np.pi*h * t)

t, r_slow, k_slow = simulate_kuramoto_dynamic(theta0, omega_f, A_all_to_all,
↪  lambda t: K_f(t, 0.01))
t, r_quasi, k_quasi = simulate_kuramoto_dynamic(theta0, omega_f,
↪  A_all_to_all, lambda t: K_f(t, 0.07))
t, r_fast, k_fast = simulate_kuramoto_dynamic(theta0, omega_f, A_all_to_all,
↪  lambda t: K_f(t, 0.2))

plt.style.use('default')
fig, (ax1, ax2, ax3) = plt.subplots(3, 1, figsize=(8, 12))

for ax, r, k, title in zip([ax1, ax2, ax3], [r_slow, r_quasi, r_fast],
↪  [k_slow, k_quasi, k_fast],
                           ['Slow variation ($h=0.01$)', 'Medium variation
                           ↪  ($h=0.07$)', 'Fast variation ($h=0.2$)']):
    ax.plot(t, r, label='r(t)', color="#0D3B6E", lw=1)
    ax_k = ax.twinx()
    ax_k.plot(t, k, label='K(t)', color="#B85C0A", lw=1, alpha=0.6, ls= '--')
    ax.set_title(title, fontsize = 11)
    ax.set_xlabel('Time $t$', fontsize = 11)
    ax.set_ylabel('Order Parameter $r(t)$', fontsize = 11)
    ax_k.set_ylabel('Coupling strength $K(t)$', fontsize = 11)

plt.tight_layout()
plt.show()
```

To generate Figure 2.7, to investigate how the topology structure affects Synchronization, we defined the following connective architectures and a function for their plotting.

```
"""
```

```
For each of the following function, the input required is the dimension
of the network and the output the relative matrix A.
"""

def topology_linear_unidirectional(N):
    A = np.zeros((N,N))
    for i in range(N-1):
        A[i+1, i] = 1
    return A

def topology_linear_bidirectional(N):
    A = np.zeros((N,N))
    for i in range(N-1):
        A[i, i+1] = A[i+1, i] = 1
    return A

def topology_box_unidirectional(N):
    A = np.zeros((N,N))
    A[1,0] = A[2,1] = A[3,2] = A[0,3] = 1
    return A

def topology_box_bidirectional(N):
    A = np.zeros((N,N))
    edges = [(0,1),(1,2),(2,3),(3,0)]
    for i,j in edges:
        A[i,j] = A[j,i] = 1
    return A

def topology_all_to_all(N):
    A = np.ones((N,N)) - np.eye(N)
    return A

def constant_K(K):
    return lambda t: K

"""
The function we now define compares the synchronization
evolution across different network
```

```
architectures for
a fixed coupling strength K. It requires:
- K: a float representing the global coupling strength;
- N: an integer representing the number of oscillators;
- T: a float for the total simulation time (default=200);
- dt: a float for the integration time step (default=0.1);
- seed: an integer to ensure reproducibility of the random natural
  frequencies and initial phases (default=0).
The function defines a set of adjacency matrices and executes a simulation
for each. It then generates a comparative plot of the order parameter r(t)
to highlight how the connectivity pattern affects the speed and
stability of synchronization.
"""

def plot_topologies(K=0.7, N=4, T=200, dt=0.1, seed=0):
    np.random.seed(seed)

    topologies = {
        "Linear uni": topology_linear_unidirectional(N),
        "Linear bi":  topology_linear_bidirectional(N),
        "Box uni":    topology_box_unidirectional(N),
        "Box bi":     topology_box_bidirectional(N),
        "All-to-all": topology_all_to_all(N)
    }

    styles = {
    "Linear uni": dict(color="#5BA3D0",lw=1,ls="-"),
    "Linear bi":  dict(color="#5BA3D0",lw=1,ls="--"),
    "Box uni":    dict(color="#B85C0A",lw=1,ls="-"),
    "Box bi":     dict(color="#B85C0A",lw=1,ls="--"),
    "All-to-all": dict(color="#0D3B6E",lw=1,ls="-"),
    }

    omega_vals = np.random.normal(0, 0.2, N)
    omega_func = lambda t: omega_vals
    theta0 = np.random.uniform(0, 2*np.pi, N)

    plt.figure(figsize=(8,5))
```

```
    plt.style.use('default')

    for name, A in topologies.items():
        t, r = simulate_kuramoto_dynamic(theta0, omega_func, A,
        ↪  constant_K(K), T=T, dt=dt)
        plt.plot(t, r, label=name, **styles[name])

    plt.xlabel("Time $t$", fontsize = 11)
    plt.ylabel("Order parameter $r(t)$", fontsize = 11)
    plt.title(f"Synchronization dynamics for different network topologies
    ↪  ($K$ = {K})", fontsize = 11)
    plt.legend(loc='lower
    ↪  right',framealpha=1,fontsize=10,edgecolor='#FFFFFF',fancybox=False)
    plt.tight_layout()
    plt.show()
```

To generate Figures 2.8 and 2.9 we used the functions `kuramoto_dynamic_step` and `simulate_Kuramoto_dynamic`, with a small but important adjustment to the coupling term. In the classical mean-field formulation of the Kuramoto model, the interaction term is normalized by the population size N. However, in this implementation the adjacency matrix already incorporates this normalization. For this reason, in the numerical simulations we omit the extra $1/N$ factor in the coupling term. This modification preserves the correct mean-field dynamics while ensuring that the numerical behavior matches the theoretical predictions.

```
"""
To generate the Gaussian Distribution figure we used the following.
"""

sigmas = [0.2, 0.5, 1.0]
N = 500
A = np.ones((N, N)) / N
K = 1.5
K_func = lambda t: K
theta0 = np.random.uniform(0, 2*np.pi, N)

plt.figure(figsize=(8,4))
plt.style.use('default')

```

```
color_map = {
    0.2: "#5BA3D0",
    0.5: "#B85C0A",
    1.0: "#0D3B6E"
}

for sigma in sigmas:
    omega_vals = np.random.normal(0, sigma, N)
    omega_func = lambda t: omega_vals
    time, r_vals = simulate_kuramoto_dynamic(theta0, omega_func, A, K_func,
    ↪  T=40, dt=0.05)

    plt.plot(time, r_vals, color = color_map[sigma], label=f"² =
    ↪  {sigma**2:.2f}", lw = 1)

plt.xlabel("Time $t$", fontsize=11)
plt.ylabel("Order parameter $r(t)$", fontsize = 11)
plt.title("Gaussian distribution: effect of variance", fontsize = 11)
plt.legend(loc='center right',fontsize = 10)
plt.tight_layout()
plt.show()

"""
To generate the Uniform Distribution figure we used the following.
"""

Rs = [0.5, 1.0, 2.0]

plt.figure(figsize=(8,4))
plt.style.use('default')

color_map = {
    0.5: "#5BA3D0",
    1.0: "#B85C0A",
    2.0: "#0D3B6E"
}

for R in Rs:
```

```
    omega_vals = np.random.uniform(-R, R, N)
    omega_func = lambda t, omega_vals=omega_vals: omega_vals
    time, r_vals = simulate_kuramoto_dynamic(theta0, omega_func, A, K_func,
    ↪  T=40, dt=0.05)
    plt.plot(time, r_vals, color=color_map[R], label=f"R = {R}", lw=1)

plt.xlabel("Time $t$", fontsize = 11)
plt.ylabel("Order parameter $r(t)$", fontsize = 11)
plt.title("Uniform distribution: effect of range", fontsize = 11)
plt.legend(loc='center right',fontsize = 10)
plt.tight_layout()
plt.show()
```

To generate Figure 2.10 we run this code.

```
N = 500
T = 100
dt = 0.05
A_all = np.ones((N, N)) - np.eye(N)
theta0 = np.random.uniform(0, 2*np.pi, N)
omega_base = np.random.normal(0, 0.5, N)
K_const = lambda t: 2.5

def omega_slow(t):
    return omega_base * (1 + 0.4 * np.sin(0.1 * t))

def omega_fast(t):
    return omega_base * (1 + 0.6 * np.sin(5.0 * t))

time_s, r_slow = simulate_kuramoto_dynamic(theta0, omega_slow, A_all,
↪  K_const, T=T, dt=dt)
time_f, r_fast = simulate_kuramoto_dynamic(theta0, omega_fast, A_all,
↪  K_const, T=T, dt=dt)

plt.figure(figsize=(8, 4))
plt.style.use('default')
plt.plot(time_s, r_slow, label='Slowly Varying $\omega_i(t)$',
↪  color="#1A6EA8", linewidth=1)
```

```
plt.plot(time_f, r_fast, label='Fast Varying $\omega_i(t)$', color="#F4913A",
↪  linewidth=1)

plt.title('Effect of Time-Dependent Natural Frequencies', fontsize=11)
plt.xlabel('Time $t$', fontsize=11)
plt.ylabel('Order Parameter $r(t)$', fontsize=11)
plt.ylim(0, 1.05)
plt.legend(fontsize=10)
plt.show()
```

To generate Figure 2.11 we used the following code.

```
N = 500
T = 300
dt = 0.05
time = np.linspace(0, T, int(T/dt))
A_all = np.ones((N, N)) - np.eye(N)
omega_base = np.random.normal(0, 0.5, N)

def omega_const(t):
    return omega_base
def omega_time(t):
    return omega_base * (1 + 0.3*np.sin(0.1*t))
def K_const(t):
    return 1.5
def K_time(t):
    return 1.5 + 0.5*np.sin(0.05*t)

cases = [
    ("K constant,  constant", K_const, omega_const,"#000000"),
    ("K(t),  constant", K_time, omega_const, "#0D3B6E"),
    ("K constant, (t)", K_const, omega_time, "#5BA3D0"),
    ("K(t), (t)", K_time, omega_time, "#B85C0A")
]

plt.figure(figsize=(8,4.8))
plt.style.use('default')

for label, K_f, omega_f, c in cases:
```

```
    theta0 = np.random.uniform(0, 2*np.pi, N)
    t_sim, r_vals = simulate_kuramoto_dynamic(theta0, omega_f, A_all, K_f,
    ↪  T=T, dt=dt)
    plt.plot(t_sim, r_vals, color=c, label=label, lw=1)

plt.xlabel("Time $t$", fontsize=11)
plt.ylabel("Order parameter $r(t)$", fontsize=11)
plt.title("Comparison between different combinations of $K(t)$ e $(t)$",
↪  fontsize=11)
plt.legend(fontsize=10)
plt.tight_layout()
plt.show()
```

Bibliography

[1] Steven H. Strogatz. "From Kuramoto to Crawford: Exploring the onset of synchronization in populations of coupled oscillators". In: *Physica D: Nonlinear Phenomena* 143 (2000), pp. 1–20.

[2] Arkadij S. Pikovsky, Michael Rosenblum, and Jürgen Kurths. *Synchronization: A Universal Concept in Nonlinear Sciences*. Cambridge, UK: Cambridge University Press, 2001.

[3] David Cumin and Christopher P. Unsworth. "Generalising the Kuramoto model for the study of neuronal synchronisation in the brain". In: *Physica D: Nonlinear Phenomena* 226 (2007), pp. 181–196.

[4] Juan A Acebrón et al. "The Kuramoto model: A simple paradigm for synchronization phenomena". In: *Reviews of Modern Physics* 77.1 (2005), p. 137.

[5] Duncan J. Watts and Steven H. Strogatz. "Collective dynamics of 'small-world' networks". In: *Nature* 393.6684 (1998), pp. 440–442.